Enhanced remediation of diesel-contaminated soils using a novel biopolymer-based emulsion

Bexultan Sabyrbay, Dorian Davarzani, Stéfan Colombano, Sagyn Omirbekov, Iliyas Kodebay, Mélanie Lorthioy, Mohamed Krimissa, Christophe Dicharry

Journal of Hazardous Materials 492 (2025) 138183

Contents lists available at ScienceDirect

Journal of Hazardous Materials

journal homepage: www.elsevier.com/locate/jhazmat

Enhanced remediation of diesel-contaminated soils using a novel biopolymer-based emulsion

Bexultan Sabyrbay [a,b,c,*], Dorian Davarzani [a], Stéfan Colombano [a], Sagyn Omirbekov [d], Iliyas Kodebay [a], Mélanie Lorthioy [b], Mohamed Krimissa [b], Christophe Dicharry [c]

[a] BRGM, F-45060, Orléans 45100, France
[b] EDF R&D, LNHE, Chatou 78400, France
[c] Université de Pau et des Pays de l'Adour, E2S UPPA, CNRS, LFCR, Pau 64013, France
[d] National Laboratory Astana, Nazarbayev University, Astana 010000, Kazakhstan

HIGHLIGHTS

- A novel alcohol-in-biopolymer emulsion achieved 100 % diesel recovery in sandy soil.
- Highly viscous shear-thinning emulsion ensured stable displacement in porous media.
- Diesel swelling induced by 1-pentanol enabled efficient mobilization and recovery.
- Porous media studies confirm complete diesel recovery with minimal fluid injection.
- Effective in direct and post-waterflooding injections with low injection pressures.

GRAPHICAL ABSTRACT

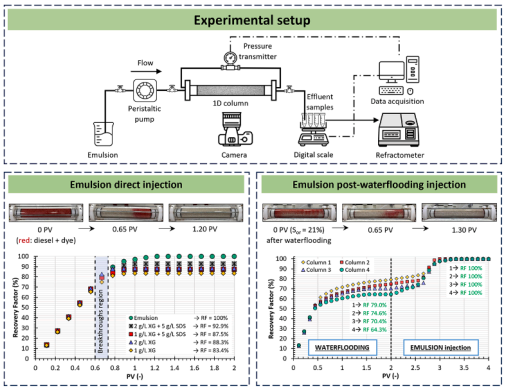

ARTICLE INFO

Keywords:
Diesel
Emulsion
Biopolymer xanthan gum
Surfactant
Oil-swelling alcohol
Porous media
Enhanced soil remediation

ABSTRACT

Conventional in-situ light non-aqueous phase liquid (LNAPL) remediation techniques often face challenges of high costs and limited efficiency, leaving residual hydrocarbons trapped in soil pores. This study investigates the efficiency of an alcohol-in-biopolymer emulsion for enhancing diesel-contaminated soil remediation. The emulsion, formulated with xanthan gum biopolymer, sodium dodecyl sulfate surfactant, and the oil-soluble alcohol 1-pentanol, was evaluated through rheological tests, interfacial tension measurements, and one-dimensional sand-column experiments under direct injection and post-waterflooding scenarios. The emulsion exhibited non-Newtonian shear-thinning behavior with high viscosity, ensuring stable propagation and efficient delivery of 1-pentanol to mobilize trapped diesel ganglia. It achieved 100 % diesel recovery within 1.2 PV during direct injection, outperforming shear-thinning polymer-only and polymer-surfactant solutions, which achieved recovery factors of 83.4–92.9 %. Post-waterflooding experiments also demonstrated 100 % diesel recovery within 1.3 PV, regardless of initial diesel saturation. Key mechanisms include reduced interfacial tension, diesel swelling and mobilization induced by 1-pentanol, and uniform displacement facilitated by the emulsion's

* Corresponding author at: BRGM, F-45060, Orléans 45100, France.
E-mail address: b.sabyrbay@brgm.fr (B. Sabyrbay).

https://doi.org/10.1016/j.jhazmat.2025.138183
Received 7 January 2025; Received in revised form 13 March 2025; Accepted 4 April 2025
Available online 7 April 2025

viscosity. Additionally, the emulsion required lower injection pressures compared to more viscous alternatives, enhancing its injectability into the soil and reducing energy demands. These findings highlight the emulsion's potential to overcome conventional remediation limitations, offering a highly effective and sustainable solution for diesel-contaminated soils and groundwater.

1. Introduction

The contamination of soils and groundwater by light non-aqueous phase liquids (LNAPLs), such as petroleum hydrocarbons, represents a significant environmental challenge due to their long-term persistence and potential carcinogenic and mutagenic risks to ecosystems and human health [77]. Upon release into the subsurface, LNAPLs infiltrate downward through the vadose zone and accumulate above the groundwater table, forming a persistent contamination source that is difficult to remediate. The conventional pump-and-treat (PT) technique is commonly used to remediate LNAPL-contaminated sites in free-phase form. However, PT often proceeds slowly and shows limited effectiveness in removing LNAPLs from the subsurface, primarily due to their physicochemical properties, such as low aqueous solubility, high interfacial tension with water, and adsorption onto soil particles [12,45]. The oil phase typically exists as ganglia within soil pores, where it is trapped by strong capillary forces that conventional methods fail to overcome [74]. Moreover, these challenges are further compounded by the complexity of the subsurface environment, particularly in heterogeneous soils, where variations in permeability and soil anisotropy hinder effective remediation [2,76]. This has led to the development of alternative in-situ remediation techniques aimed at enhancing contaminant removal from subsurface environments.

Several alternative in-situ remediation approaches have been explored to enhance the recovery of LNAPLs from subsurface environments. Among these approaches, surfactant-enhanced aquifer remediation (SEAR) [9,25,39,41,42,59,84] and cosolvent (i.e., alcohol) flushing [22,32,38] have shown promise in removing contaminants from soil pores. Surfactant-induced displacement of LNAPLs has been shown through two primary mechanisms: (i) mobilization, driven by a reduction in the LNAPL/water interfacial tension (IFT), and (ii) micellar solubilization, wherein LNAPL droplets are incorporated within surfactant micelles [30,31]. The micellar solubilization typically occurs at surfactant concentrations exceeding the critical micelle concentration, resulting in the formation of a Winsor Type I microemulsion system.

Similarly, alcohol flushing can enhance both the mobilization and solubilization mechanisms of LNAPL trapped in soil pores [22,32,44]. The displacement mechanisms can vary depending on the specific type of alcohol (e.g., molecular weight) used in the flushing solution and the distinct properties of LNAPL. Lower molecular weight alcohols, typically those lighter than four carbon atoms (C_4), are generally water-soluble and act as cosolvents, reducing the polarity of the water phase and making it more compatible with LNAPL. This reduces the IFT between water and LNAPL, enabling the dissolution of LNAPL without requiring the presence of surfactants at micellar concentrations [3,32,38]. For instance, [63] demonstrated that a surfactant-alcohol solution (3 % Brij-97 with 2.5 % n-pentanol "cosolvent") achieved over 90 % of residual NAPL removal within 8–10 pore volumes via in-situ microemulsion formation, relying on a solubilization mechanism rather than mobilization. Similarly, [68] investigated polymer-enhanced surfactant flushing, where a solution of 4 g/L xanthan gum (XG) and 2.3 g/L sodium dodecyl sulfate (SDS) led to remarkable petroleum hydrocarbon removal within 5 pore volumes in a glass micromodel, as assessed by image analysis (though the exact recovery factor was not specified). Their approach also relied on the in-situ microemulsion formation, employing a solubilization mechanism to enhance NAPL dissolution and transport. Likewise, [21] employed in-situ microemulsion formation for NAPL solubilization and displacement, using high surfactant concentrations (4–8 %) in combination with isopropanol as a cosolvent and xanthan gum as a viscosifier. Moreover, incorporating surfactants and alcohols into a single flushing fluid as microemulsions has been proven to significantly enhance LNAPL removal within porous media [8,29]. Their application achieves ultra-low IFT between immiscible phases and alters the wettability of the soil matrix, thereby enhancing the desorption, aqueous apparent solubility, and subsequent mobilization of contaminants previously adsorbed onto soil particles.

Nevertheless, remediation methods based on solubilization mechanisms are generally less efficient for NAPL removal compared to those employing mobilization mechanisms [21,31,69]. Enhanced NAPL removal can often be achieved with mobilization mechanisms in just a few pore volumes of fluid flushing, whereas solubilization-dominated remediation typically requires tens to hundreds of pore volumes, thereby increasing flushing costs [21,69]. The presence of higher molecular weight alcohols ($>C_4$) in the flushing fluid can further enhance the mobilization mechanism by swelling or expanding the NAPL phase. These longer-chain alcohols preferentially partition into the NAPL phase rather than the aqueous phase, due to their lower polarity and strong affinity for NAPLs [28,71]. Through this partitioning and subsequent swelling, residual NAPL ganglia are transformed into a continuous phase within porous media, becoming less dense and less viscous, which significantly improves their mobilization compared to discontinuous NAPL residues [11]. Notably, the application of these "oil-swelling" or "NAPL-swelling" alcohols has predominantly targeted dense non-aqueous phase liquids (DNAPL) [11,34,44,62,71,73]. In contrast, only one study assessed the effectiveness of oil-swelling alcohols in removing LNAPLs. In that study, [32] investigated the swelling behavior of benzene residues (LNAPL) using a two-dimensional glass pore network micromodel measuring 15 cm× 10 cm. Their experiments demonstrated that injecting 30 % tert-butanol or 30 % 1-propanol caused swelling of benzene residues. Moreover, the co-injection of air with the flushing solution significantly improved benzene removal by facilitating LNAPL mobilization through the swelling mechanism. However, their study was conducted in a homogeneous porous medium, whereas in a heterogeneous systems, surfactant or cosolvent injection alone may be ineffective due to bypassing of low-permeability zones, where LNAPL droplets may remain trapped [72,67]. Similarly, air co-injection with cosolvents injection may induce preferential flow through high-permeability pathways, further reducing displacement efficiency in low-permeability regions. Moreover, high-pressure airflow injection may cause soil damage, including cracking or fissuring, potentially leading to unintended subsurface flow pathways and compromised remediation efficiency [54].

Despite advancements in in-situ flushing methods, their efficiency is significantly reduced in heterogeneous soils with high anisotropy, posing challenges in cost and long-term effectiveness. In recent years, attention has shifted towards using viscous shear-thinning fluids, such as aqueous foam [5,6,24,33,43,56,57] and polymer solutions [26,48,68], to enhance LNAPL recovery from the subsurface. The shear-thinning behavior of these fluids enable to prevent bypassing of low-permeability zones in heterogeneous porous media, ensuring stable and uniform displacement [10]. Aqueous foams have been increasingly studied for their potential in LNAPL remediation due to their ability to reduce interfacial tension and enhance displacement efficiency in porous media. However, despite their broad capabilities, maintaining foam stability in the presence of petroleum hydrocarbons remains a significant challenge, as it impacts on foam properties (e.g., viscosity) and behavior (e.g., rheology, increased collapsing time). In contrast, polymer solutions do not encounter such stability challenges in

hydrocarbon-contaminated environments. Although relatively few studies have explored the use of polymers for LNAPL removal from soil [26,49,64,68,87], findings indicate that recovery yields achieved with polymer solutions are significantly higher than those obtained with conventional PT methods. However, even after polymer flushing, some LNAPL ganglia may remain trapped in the soil pores, rendering them immobile. In addition, the use of high-viscosity fluids presents certain challenges, such as increased injection pressure, which can lead to injection difficulties or even soil uplift [55].

To overcome these limitations, polymer solutions can be combined with other in-situ remediation techniques within a single flushing fluid to enhance sweeping efficiency. [85,86,88] reported that xanthan gum-based polymer solutions significantly improve the transport of remedial agents into low-permeability zones in heterogeneous porous media, thereby enhancing sweep efficiency. Meanwhile, [7] demonstrated that a xanthan gum-ethanol mixture, injected into a heterogeneous soil column composed of silica sand (92 %), clay (5 %), and organic matter (3 %), propagated uniformly throughout the porous medium, effectively facilitating ethanol transport. Similarly, [78] and [1] showed that xanthan-based mixtures successfully overcame soil heterogeneity, maintaining stable and uniform displacement in multilayer soil systems with high permeability contrast. Despite these advancements, the use of oil-swelling alcohols for LNAPL remediation remains largely unexplored, with only one study reported to date [32]. This research gap is likely due to the similarities in physical properties between oil-swelling alcohols and LNAPLs, which may have limited their application despite their promising potential for enhancing LNAPL removal. Furthermore, direct alcohol injection may not be applicable in heterogeneous soil systems, as alcohols tend to preferentially flow by high-permeability pathways, bypassing low-permeability regions and reducing overall remediation efficiency. To address this research gap, our study introduces an alcohol-in-biopolymer (oil-in-water) emulsion as a novel flushing fluid to enhance LNAPL remediation efficiency. The proposed emulsion is formulated with xanthan gum (XG) biopolymer, oil-soluble 1-pentanol, and the environmentally friendly surfactant sodium dodecyl sulfate (SDS). This formulation incorporates the biopolymer-stabilized emulsion's ability to enhance the transport of dispersed 1-pentanol droplets into low-permeability regions, while the oil-swelling properties of 1-pentanol facilitate LNAPL swelling and displacement, ultimately improving overall remediation efficiency.

This study has two main objectives: (i) to quantitatively evaluate the emulsion's performance in LNAPL removal under direct injection and post-waterflooding scenarios through one-dimensional sand-packed column experiments, while comparing its efficiency with other shear-thinning polymer and polymer-surfactant solutions; and (ii) to explore the underlying mechanisms governing emulsion's behavior during injection. To this end, bulk experiments, including rheological and interfacial tension measurements, were conducted to examine the emulsion's rheological behavior and its LNAPL displacement mechanisms in porous media. The LNAPL recovery was determined by measuring the refractive index of the organic phase in the effluent (see Section 2.7). This method is original, rapid and easier to implement compared to generally used techniques, in particular gas chromatography with a flame ionization detector (GC-FID).

2. Materials and methods

2.1. Soil and LNAPL contaminant

The porous medium used in this study consisted of extra-siliceous sand supplied by Sibelco, with grain sizes (D_g) ranging from 0.4 to 1.5 mm (D_{50} = 1.0 mm). This silica sand was chosen to replicate the properties of a contaminated plurimetric-scale setup (BRGM's PRIME platform in Orléans, France), including its grain size, permeability, and porosity.

The LNAPL used in this study was diesel fuel supplied by TotalEnergies. To enhance its visualization within the porous media, Oil-Red-O, an oil-soluble dye from Sigma-Aldrich, was added to the diesel at a concentration of 0.2 g/L. The addition of the dye did not significantly change the physical properties of the diesel. The measured physical properties of the diesel are summarized in Table 1.

2.2. Emulsion components

Xanthan gum (XG), a water-soluble anionic biopolymer derived from *Xanthomonas campestris*, was selected as the base for the aqueous phase of the emulsion due to its viscous, shear-thinning properties [18,52,53,55]. The XG was supplied in dry powder form by Sigma-Aldrich.

1-pentanol, an oil-soluble alcohol, was used as the oil phase of the emulsion for its ability to swell diesel, as highlighted by [66]. Furthermore, 1-pentanol is known for its biodegradability [4,75], making it an environmentally favorable choice for remediation applications. The 1-pentanol (≥99 % purity) was provided by Sigma-Aldrich, and its physical properties are listed in Table 1.

Sodium dodecyl sulfate (SDS), a biodegradable and environmentally friendly surfactant [47], was chosen for its dual role as both a surfactant and an emulsion stabilizer. Its anionic nature plays a crucial role in emulsion stabilization by promoting electrostatic repulsion between dispersed droplets, thereby preventing coalescence [19]. Additionally, SDS exhibits low adsorption onto silica soil surfaces due to their similar negative charge, which helps maintain surfactant availability in the system. SDS, with a purity of ≥ 98.5 %, was supplied in dry powder form by Sigma-Aldrich.

Deionized water with a resistivity of 18.2 MΩ.cm, produced using a Milli-Q water purification system, was used for preparing all aqueous solutions and throughout all aspects of the experimental study.

2.3. Emulsion preparation

The aqueous phase of the emulsion was prepared by dissolving SDS powder in deionized, degassed water and stirring for 3 h at 300 rpm. The SDS concentration was set at 5 g/L, which is approximately twice its critical micelle concentration of 8.2 mM (2.3 g/L) [65]. This concentration was selected to provide surfactant depletion may occur due to adsorption onto silica particles. Once SDS was fully dissolved, XG powder was gradually added to the solution at a concentration of 1 g/L and stirred for 12 hours at 300 rpm to avoid agglomeration and achieve uniform dispersion. The 1 g/L XG concentration was chosen based on [40] to ensure stable displacement behavior within porous media with a grain size range of 0.4–1.5 mm at a displacement velocity of 1 m/day. The emulsion was then prepared by mixing the aqueous polymer-surfactant phase with the organic 1-pentanol phase in a 1:1 vol ratio. The mixture was homogenized using an overhead stirrer (DLAB OS40-S; Servilab, France) at 500 rpm for 3 h to ensure proper emulsion formation.

2.4. Bulk rheological measurements

The rheological behavior of the emulsion was analyzed using a Haake Mars 60 rheometer (Thermo Fisher Scientific) at a controlled temperature of 20°C. Measurements were performed with parallel plate-plate geometry (P60/Ti and TMP60), ensuring precise sample placement and proper filling of the gap between the plates. Viscosity measurements were conducted across a range of controlled shear rates from 0.01 s^{-1} to 100 s^{-1}, with steady-state viscosity values recorded at each shear rate.

To evaluate the rheological advantage of forming an emulsion, its rheological behavior was compared to that of its continuous phase, an aqueous solution containing 1 g/L XG and 5 g/L SDS. Additionally, the study examined the rheology of various polymer solutions used in the experiments, including (i) 1 g/L XG, (ii) 2 g/L XG, and (iii) 2 g/L XG with 5 g/L SDS. All measurements were conducted in triplicate to ensure reliability and reproducibility of the results.

Table 1
Physical properties of fluids at 20°C.

Fluid	Density, ρ (g/cm^3)	Dynamic viscosity, μ (mPa.s)	Fluid/deionized water interfacial tension, σ (mN/m)	Refractive index at wavelength λ= 589 nm, *RI* (-)
Diesel oil	0.824 ± 0.001	3.15 ± 0.05	21.8 ± 0.1	1.45520 ± 0.00001
1-pentanol	0.811	3.441	4.2 ± 0.1	1.40787 ± 0.00001

The viscosity data for all fluids were plotted as a function of shear rate to evaluate their rheological behavior. The Carreau-Yasuda model [80] was applied to fit the experimental rheological curves, where the apparent viscosity μ (Pa.s) at a given shear rate $\dot{\gamma}$ (s^{-1}) is expressed as:

$$\mu(\dot{\gamma}) = \mu_\infty + (\mu_0 - \mu_\infty)[1 + (\lambda\dot{\gamma})^a]^{\frac{n-1}{a}} \quad (1)$$

where, μ_0 (Pa.s) is the zero-shear viscosity, μ_∞ (Pa.s) are the infinite-shear viscosity, n (−) is the power-law index, a (-) is the transition parameter, and λ (s) is the time constant that defines the transition from the Newtonian region to the power-law region of flow.

2.5. Interfacial tension measurements

The primary objective of measuring the interfacial tension (IFT) was to evaluate the impact of 1-pentanol and the SDS surfactant on the IFT between the aqueous polymer-surfactant phase and the organic diesel phase. Furthermore, understanding IFT behavior is essential for assessing emulsion stability and the efficiency of fluid displacement in porous media. In this study, IFT was measured across various interfaces, including deionized water or polymer solutions (1 g/L or 2 g/L XG) with diesel or 1-pentanol, as well as polymer-surfactant solutions (1 g/L or 2 g/L XG with 5 g/L SDS) with diesel, 1-pentanol, or a 1:1 vol mixture of 1-pentanol and diesel.

The IFT measurements were conducted using a DSA-100 Drop Shape Analyzer (KRÜSS) with the pendant drop method [70]. A clean syringe and needle were used to form a pendant drop of the aqueous phase. The syringe, filled with the aqueous phase, mounted on the apparatus. A pendant drop was gradually formed at the needle tip, which was immersed in a glass cuvette filled with 6 mL of the organic phase. The aqueous phase was dosed carefully until the drop reached a sufficient size for analysis. The images of the drop were captured by the apparatus's camera, and the IFT was calculated automatically using the Young-Laplace equation. All measurements were conducted at 20°C and repeated five times to ensure accuracy and reproducibility.

2.6. Experimental study in porous media

The primary objective of the one-dimensional (1D) column experiments was to evaluate the effectiveness of the emulsion in removing diesel from a porous medium (silica sand-pack).

2.6.1. Experimental setup

A conceptual illustration of the 1D-column experiment setup is presented in Fig. 1. The column, made of a glass tube with an internal radius of 4 cm and a length of 30 cm, was designed for experiments involving an unconsolidated sand-pack. Two metallic mesh grids with a pore size of 250 μm were placed at either end of the column to retain the sand. All fluids were injected into the sand-pack using a Reglo ICC Ismatec® digital peristaltic pump, offering a resolution of 0.01 rpm. Differential pressure along the column was measured using a Rosemount 3051S Emerson transmitter, with a range of 0–625 mbar (± 5 mbar at maximum pressure). Effluent samples were collected in 15 mL polypropylene tubes and monitored using a Scout STX6201 OHAUS® digital scale (6200 g capacity, 0.1 g precision). The concentration of diesel in the effluent samples was determined by measuring the refractive index using an Abbemat Performance Plus 550 (Anton Paar®) digital refractometer, with an accuracy of ± 0.00002 nD and a resolution of ± 0.000001 nD (see Section 2.7).

2.6.2. Experimental procedure

The installation and preparation of the 1D column were carried out according to the following protocol. First, the sand was thoroughly washed with demineralized water to remove dust, which could affect the permeability of the sand-pack. It was then dried in an oven at 95°C for two days. The glass column was first positioned vertically and packed with the dried sand to create an unconsolidated porous medium. Once filled with sand, the column was pressurized to 3 bar using air, and the pressure was monitored for over one hour to check for leaks. Afterward, the column was flushed with CO_2 at a flow rate of 3 mL/min for one hour to remove trapped air, as the solubility of CO_2 in water prevents the formation of air bubbles within the porous medium. Subsequently, the column was saturated from bottom to top with three pore volumes of degassed, deionized water at a constant flow rate of 1 mL/min. The mass of the column was measured both before and after water saturation to calculate the pore volume (PV) and porosity of the porous medium. After achieving uniform water saturation, the column was positioned horizontally to measure the intrinsic permeability (k). This was determined by injecting deionized water at flow rates ranging from 1 to 10 mL/min while measuring the resulting pressure drop along the column. The permeability (k) was then calculated using Darcy's law, as follows:

$$u = \frac{Q}{A} = \frac{k\Delta P}{\mu L} \quad (2)$$

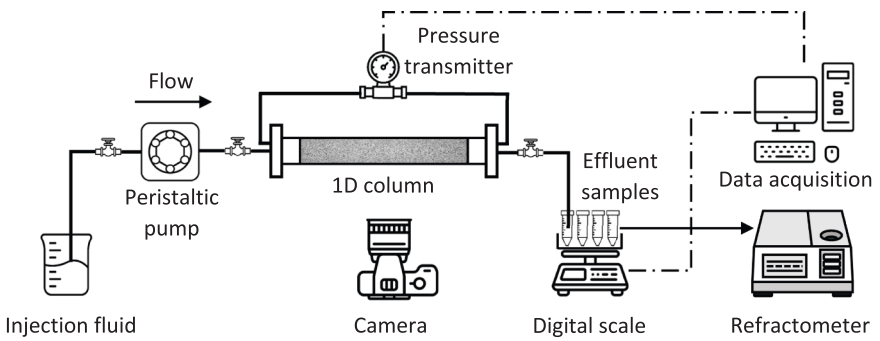

Fig. 1. Schematic diagram of the experimental setup for diesel recovery via emulsion injection in a 1D sand-pack column.

where, u (m/s) is the Darcy velocity, Q (m^3/s) is the flow rate, A (m^2) is the cross-sectional surface area of the porous medium, k (m^2) is the intrinsic permeability, ΔP (Pa) is the pressure drop along the length L (m), and μ (Pa.s) is the dynamic viscosity of the fluid, which can be defined as follows for Newtonians fluids,

$$\mu = \frac{\tau}{\dot{\gamma}} \tag{3}$$

where, τ (Pa) is the shear stress and $\dot{\gamma}$ (s^{-1}) is the shear rate. Consequently, the equivalent shear rate ($\dot{\gamma}_{eq}$) within porous media can be determined using the equation proposed by [17]:

$$\dot{\gamma}_{eq} = \frac{4\alpha u}{\varnothing r_{eq}} \tag{4}$$

where, α represents a shift factor influenced by the tortuosity of the porous media with the porosity $\varnothing$ (-) and the rheological properties of the bulk fluid, as described by [13]. Based on the mathematical derivation representing the porous media as a bundle of capillaries, in accordance with the Darcy's and Poiseuille's laws, the mean pore radius r_{eq} (m) can be calculated using the Kozeny [35] equation as follows:

$$r_{eq} = \sqrt{\frac{8k}{\varnothing}} \tag{5}$$

In the subsequent stage, the water-saturated sand-pack was positioned vertically, and diesel was introduced at a constant flow rate of 1 mL/min until irreducible water saturation (S_{wi}, %) was reached. The diesel was injected in a top-down direction to avoid gravitational effects and prevent fingering caused by density differences. The irreducible water saturation was determined by measuring the volume of water present in the effluent. Table 2 lists the main measured properties of the porous media used in this study.

Diesel recovery experiments were conducted using a horizontally positioned column to mimic reservoir conditions, with all fluid injections performed at a fixed flow rate of 1 mL/min. Two fluid injection methods (direct treatment and post-treatment) were employed to assess the effectiveness of the emulsion in removing diesel from the sand-pack:

i. *Direct treatment* experiments involved injecting 2 PV of the emulsion immediately after saturating the column with diesel. This method aimed to displace the continuous phase of diesel in the porous medium through direct fluid injection. Additionally, the efficiency of the emulsion was compared with aqueous polymer-only solutions (1 g/L XG and 2 g/L XG) and polymer-surfactant solutions (1 g/L XG + 5 g/L SDS and 2 g/L XG + 5 g/L SDS). All direct treatment experiments were performed in triplicate to ensure reproducibility of the results.

ii. *Post-treatment* experiments involved applying a waterflooding (WF) process designed to mimic the conventional pump-and-treat technique, followed by emulsion injection. The WF process consisted of injecting 2 PV of deionized and degassed water into the diesel-saturated column to achieve residual diesel oil saturation (S_{or}, %). Subsequently, 2 PV of the emulsion were injected to assess its effectiveness in removing residual diesel. All post-treatment experiments were carried out in quadruplicate.

2.7. Effluent analysis

Effluent mass and volume measurements were used in immiscible fluid displacement experiments (without the presence of 1-pentanol) to estimate diesel recovery. In contrast, for miscible fluid displacement experiments, refractive index analysis of the organic phase in the effluent was performed alongside mass and volume measurements to quantify diesel recovery. Prior to refractive index measurements, the effluent samples were centrifuged at 5000 rpm for 20 min using a Sigma 3–16PK centrifuge to separate the aqueous phase (XG + SDS solution) from the organic phase (a mixture of diesel and 1-pentanol). The volumes of the separated organic and aqueous phases were measured and recorded. The refractive index of the organic phase was then measured by placing 0.2–0.5 mL of the sample onto the glass prism of the refractometer. The diesel volume fraction φ_d (-) in the organic phase was determined from the measured refractive index n (-) using a calibration curve (Eq. (6)), which was previously constructed using a set of standard solutions with varying volume fractions of diesel and 1-pentanol (see Supporting Data S1).

$$n = 0.047\varphi_d + 1.4076 \tag{6}$$

3. Results and discussion

3.1. Bulk characterization of emulsion

3.1.1. Emulsion rheological behavior

Fig. 2 presents the viscosity profiles of the emulsion and various polymeric solutions as a function of shear rate at 20°C. All systems, including XG solutions at concentrations of 1 g/L and 2 g/L, as well as XG + SDS solutions (1 g/L XG + 5 g/L SDS and 2 g/L XG + 5 g/L SDS), exhibit non-Newtonian shear-thinning behavior, characterized by a decrease in viscosity (μ) with increasing shear rate ($\dot{\gamma}$). Similarly, the emulsion, comprising a continuous aqueous phase of 1 g/L XG + 5 g/L SDS and a dispersed organic phase of 1-pentanol at a 1:1 vol ratio, also demonstrated shear-thinning behavior across a wide range of shear rates.

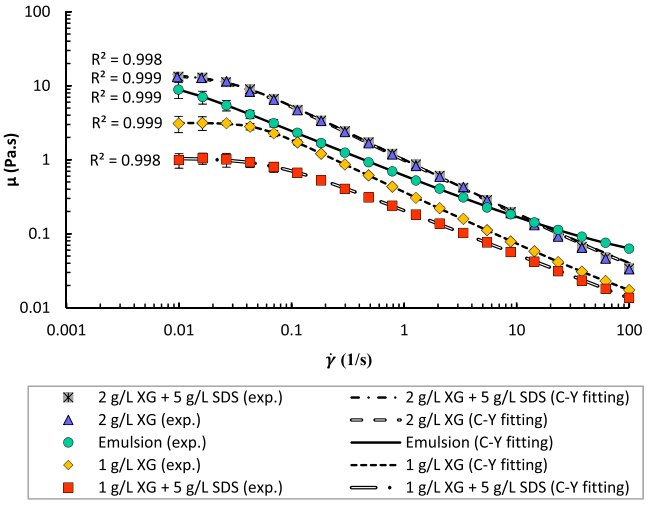

Fig. 2. Viscosity as a function of shear rate for various fluids with Carreau-Yasuda model fitting curves.

Table 2
Properties of porous medium.

Porous media	Grain size diameter, d (mm)	Porosity, $\varnothing$ (%)	Permeability, k (m^2)	Pore Volume, PV (mL)	Mean pore radius, r_{eq} (μm)	Irreducible water saturation, S_{wi} (%)
Silica sand	0.4–1.5	36 ± 0.5	270 (± 20) × 10^{-12}	137 ± 1.0	79 ± 2.2	17 ± 0.5

Notably, the emulsion maintained shear-thinning rheology even at low shear rates (0.01–0.04 s^{-1}), whereas all polymeric solutions demonstrated a Newtonian plateau in this range. This Newtonian plateau can be attributed to the formation of three-dimensional networks created by the entanglement of XG chains at low shear rates, which gradually break down as the shear rate increases [83]. At higher shear rates (15–100 s^{-1}), the emulsion with 1 g/L XG in its continuous phase exhibited a higher viscosity compared to aqueous polymer solutions containing twice the XG concentration (2 g/L). To further characterize these rheological behaviors, the experimental data were fitted using the Carreau-Yasuda (C-Y) model (see Eq. (1)), which demonstrated excellent agreement with the experimental data, as indicated by high coefficients of determination ($R^2 > 0.99$). The fitting parameters obtained via nonlinear regression are summarized in Table S. 1 (see Supporting Data S2).

While all fluids demonstrate shear-thinning rheology, notable differences are observed in their viscosity profiles. The viscous behavior is primarily attributed to the presence of XG polymer in various fluid mixtures, with the viscosity of XG solutions increasing at higher polymer concentrations. However, the addition of 5 g/L SDS to the 1 g/L XG solution resulted in a reduction in overall viscosity, likely due to conformational changes in XG molecules caused by their interaction with SDS. This viscosity reduction can be attributed to phenomena such as electrostatic repulsion between similarly charged XG and SDS molecules [1,36], hydrophobic interactions, hydrogen bonding, and the formation of mixed micelles [82]. SDS modifies the stretched state of XG molecules in solution, causing the polymer chains to twist and shrink, which disrupts the polymer network structure and subsequently reduces viscosity. Additionally, SDS may induce wall-slip effects during viscosity measurements by creating a slip velocity between the solution and the parallel plates, thus affecting the true shear values [57].

At higher XG concentrations (2 g/L), the addition of SDS (5 g/L) had little impact on viscosity, as the viscosity profiles of 2 g/L XG and 2 g/L XG + 5 g/L SDS were nearly similar. This suggests that the dense and entangled polymer chain network dominates the rheological behavior, making the system less sensitive to SDS-induced disruptions [51].

Interestingly, a different trend is observed for the emulsion formed by combining oil-soluble 1-pentanol with an aqueous solution containing 1 g/L XG and 5 g/L SDS. At a shear rate of 1.86 s^{-1}, which corresponding to flow through a porous medium at an injection flow rate of 1 mL/min (calculated using Eq. (4)), the emulsion's viscosity was three times greater than that of its continuous phase (1 g/L XG + 5 g/L SDS) and 1.8 times greater than that of the XG solution alone at the same polymer concentration (1 g/L). Furthermore, the relative viscosity for this emulsion, defined as the ratio μ_{0em}/μ_{0c}, was approximately 12, where μ_{0em} and μ_{0c} represent the zero-shear viscosities of the emulsion and its continuous phase, respectively. These values were determined at zero-shear rates using the Carreau-Yasuda model (see Supporting Data S2 for details).

The high relative viscosity is primarily attributed to the dispersed oil droplets (1-pentanol), which introduce additional flow resistance, thereby increasing the system's viscosity. At a 1:1 vol ratio, the dispersed 1-pentanol droplets occupy a significant space within the emulsion, hindering the motion of the continuous phase [58]. Additionally, the densely packed droplets form an internal network with strong inter-droplet interactions, further enhancing the emulsion's structural complexity [81]. Such interactions are common in emulsions with high dispersed phase content and are known to contribute to increased viscosity and non-Newtonian shear-thinning behavior, as noted by [50]. Consequently, this increase in viscosity highlights the emulsion' potential for enhanced LNAPL removal in porous media, as higher viscosity fluids with shear-thinning behavior can significantly improve sweep efficiency and displacement performance.

3.1.2. Interfacial tension

The interfacial tension (IFT) measurement results between the aqueous and organic phases are presented in Table 3. The IFTs between XG solutions (at both 1 g/L and 2 g/L) and diesel were lower than those observed for deionized water alone with diesel. Moreover, the IFT decreased with increasing XG concentration in deionized water. The incorporation of SDS surfactant (5 g/L) into XG solutions at 1 g/L and 2 g/L led to a significant reduction in IFT, decreasing it by more than twelvefold in both cases. These findings align closely with those reported by [1], who observed a fourteenfold IFT reduction when incorporating sodium dodecyl benzene sulfonate (SDBS) surfactant into XG solutions.

The IFT between deionized water (with and without XG) and 1-pentanol was notably over five times lower than that between deionized water and diesel. Similarly, the IFT between the emulsion's continuous phase (an aqueous solution containing 1 g/L XG and 5 g/L SDS) and the dispersed phase (1-pentanol) was comparable to the IFT between the aqueous solution of 1 g/L XG with 5 g/L SDS and diesel. A slight reduction in IFT was observed between the aqueous phase of the emulsion and the diesel/1-pentanol mixture at 1:1 vol ratio. These IFT measurements were subsequently employed to estimate the diesel displacement regimes for various injection fluids within porous media.

3.2. Characterization of injection fluids in porous media

The displacement regimes of immiscible fluid flow within porous media are characterized by the interplay between capillary and viscous forces. Depending on which force predominates, the displacement can manifest as: (i) capillary fingering, (ii) viscous fingering, or (iii) stable displacement [40,61]. These regimes are typically characterized using dimensionless numbers, such as the capillary number (Ca) and the viscosity ratio (M), which describe the relative influence of viscous and capillary forces on the displacement process [27,55]. These parameters are defined as follows,

$$Ca = \frac{\mu_d u}{\sigma} \tag{7}$$

$$M = \frac{\mu_r}{\mu_d} \tag{8}$$

where, u (m/s) is the Darcy velocity, σ (N/m) is the interfacial tension between two immiscible fluids, μ_d (Pa.s) and μ_r (Pa.s) are the displacing and resident fluid dynamic viscosities, respectively.

The phase diagram proposed by Lenormand et al. [40], which plots the logarithm of the capillary number (log(Ca)) against the logarithm of the viscosity ratio (log(M)), was used to characterize the diesel displacement regimes within porous media for various injection fluids, including emulsion, water, and aqueous polymeric solutions with and without SDS. For the emulsion, Ca was calculated using: (i) the IFT value of 1.64 mN/m, determined between the resident diesel and the emulsion's continuous phase (an aqueous solution containing 1 g/L XG with 5 g/L SDS, as shown in Table 3), and (ii) the emulsion's bulk viscosity of 0.44 Pa.s, measured at a shear rate of 1.86 s^{-1}, which corresponds to the shear rate in porous media at an injection flow rate of 1 mL/min.

Table 3
Interfacial tension (IFT) of different pairs of fluid.

Aqueous phase	IFT with diesel (mN/m)	IFT with 1-pentanol (mN/m)	IFT with diesel/1-pentanol at 1:1 vol ratio (mN/m):
Deionized water	21.8 ± 0.1	4.2 ± 0.1	5.2 ± 0.1
1 g/L XG	19.8 ± 0.1	3.9 ± 0.1	-
2 g/L XG	17.6 ± 0.1	-	-
1 g/L XG + 5 g/L SDS	1.6 ± 0.1	1.6 ± 0.1	1.3 ± 0.1
2 g/L XG + 5 g/L SDS	1.2 ± 0.1	-	-

Moreover, *M*, defined as the ratio of the emulsion's bulk viscosity to that of the resident diesel, was used to assess the displacement dynamics. The shear rate in porous media was determined using Eq. (4), and the parameters used to calculate *Ca* and *M* for each displacing fluid are summarized in Table S. 2 (see Supporting Data S4).

According to Lenormand's phase diagram, log(*Ca*) values were negative for all injecting fluids, while log(*M*) values were positive for all except deionized water. These values placed all fluids within the transition zone between the capillary fingering and stable displacement zones. This positioning indicates a complex displacement behavior, characterized by intermittent capillary fingering alongside a more stable displacement front. The transitional regime is influenced by various factors, including pore geometry, fluid properties, and injection parameters, suggesting the complex nature of the displacement process [23]. Meanwhile, the positive logarithmic values of the viscosity ratios confirm the absence of viscous fingering, indicating a predominantly stable displacement regime across all cases. Notably, the phase diagram also highlights the unique position of deionized water (blue cross), which falls firmly within the capillary fingering zone due to its low viscosity and high IFT relative to diesel. Comparable positionings were reported in the microfluidic experiments by [79], the glass bead column studies by [16], and the low-permeability soil experiments conducted by [23]. The low *Ca* and *M* for deionized water confirm its limited effectiveness in achieving stable displacement, leading to inefficient diesel recovery. This stark contrast underscores the importance of incorporating viscous and IFT-reducing additives, such as polymers and surfactants/alcohols, to enhance displacement efficiency and shift the regime closer to stable displacement zones.

The phase diagram reveals that fluids with lower polymer concentrations, such as the 1 g/L XG solution (yellow diamond), fall within the transition zone and exhibit a less stable displacement front compared to higher-concentration solutions. Similar positioning in the transition zone was observed by [55] for a 1 g/L XG solution used to displace chlorinated solvents (DNAPL) in glass bead-packed columns. Increasing the polymer concentration, as in 2 g/L XG solution (blue triangle), shifts the displacement regime closer to the stable zone. The addition of SDS (5 g/L) to XG solutions (red square and black cross) significantly improves displacement performance by reducing interfacial tension and increasing capillary number, placing these fluids firmly closer to the stable displacement region.

The emulsion (green circle) demonstrates superior displacement efficiency compared to the 1 g/L XG, 2 g/L XG, and 1 g/L XG + 5 g/L SDS solutions, as it is positioned closer to the stable displacement regime. This improved performance is attributed to the emulsion's combination of high viscosity and low interfacial tension, which optimizes the balance between capillary and viscous forces, promoting more uniform displacement with minimal fingering. However, the 2 g/L XG + 5 g/L SDS solution (black cross) is positioned above the emulsion, closer to the stable displacement zone. With increasing XG concentration, the solution exhibits higher viscosity (see Fig. 2), which improves mobility control by reducing the risk of viscous and capillary fingering. Therefore, the increased viscosity improves sweep efficiency, ensuring a more uniform displacement of the diesel phase. Additionally, the presence of SDS further reduces IFT, facilitating diesel mobilization and enhancing overall displacement efficiency. This suggests that the synergistic effects of a higher polymer concentration combined with SDS further enhance displacement stability and efficiency in porous media.

Nevertheless, it is worth noting that the emulsion's diesel swelling capability is not accounted for in Lenormand's phase diagram. This unique phenomenon is further explored through column experiments to gain a deeper understanding of its impact on diesel displacement.

3.3. Assessment of diesel recovery efficiency in one-dimensional porous media

3.3.1. Impact of direct emulsion injection on diesel recovery

Fig. 4a depicts the diesel removal efficiency results via direct injection for the emulsion and various XG solutions (1 and 2 g/L) with and without SDS (5 g/L) as a function of PV. The irreducible water saturation in all sand-pack columns was approximately 17 ± 0.5 %. Breakthroughs for 1 g/L and 2 g/L XG solutions occurred at 0.6 PV and 0.65 PV, respectively. For the 1 g/L XG + 5 g/L SDS and 2 g/L XG + 5 g/L SDS

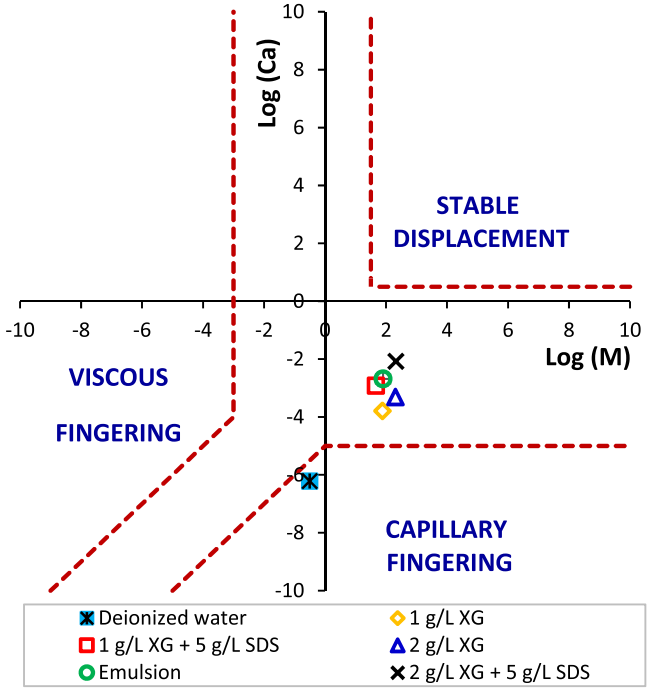

Fig. 3. Comparison of diesel displacement regimes in porous media for emulsion and various polymer and polymer-surfactant solutions using Lenormand's phase diagram.

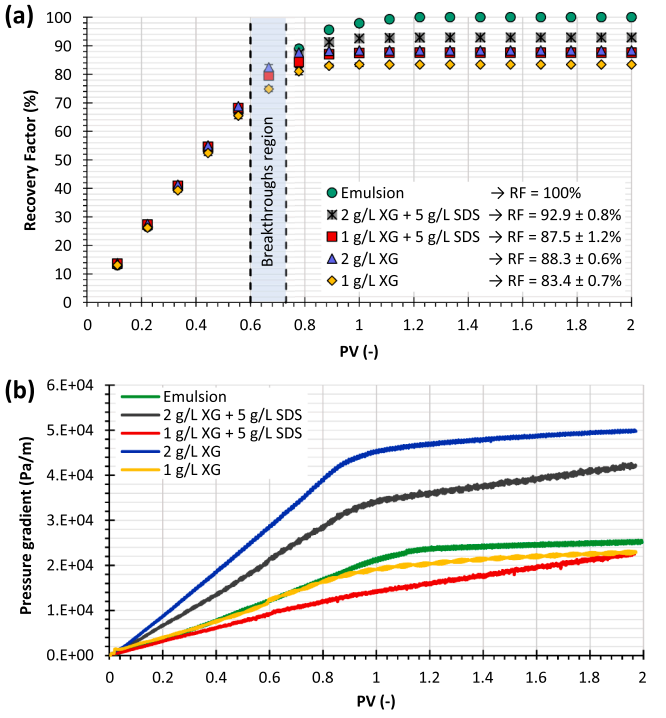

Fig. 4. Direct fluid injection as a function of PV in porous column: (a) recovery factors, and (b) pressure gradient evolutions.

solutions, breakthroughs were observed at 0.63 PV and 0.67 PV, respectively, demonstrating a slight delay due to the presence of SDS. This delay is likely attributed to the reduced IFT between the aqueous and organic phases, which increases diesel mobilization. In contrast, the emulsion exhibited a breakthrough at 0.73 PV, indicating its more complex displacement dynamics compared to the other fluids.

The evolution of the recovery factors (RF) follows three distinct phases, corresponding to the two-phase flow behavior in porous media, which occurs as a piston-like flow within a stable displacement. Initially, at around 0.6 PV, all injection fluids exhibit comparable RF values, achieving approximately 70 % recovery with no significant differences between them. Beyond this point, in the range of 0.6 – 1.2 PV (after breakthrough), the nature of each injected fluid becomes a significant factor in diesel removal efficiency. Increasing the polymer (XG) concentration correlates with improved RF, reaching 83.4 ± 0.7 % and 88.3 ± 0.6 % for XG concentrations of 1 g/L and 2 g/L, respectively. Incorporating SDS surfactant into XG solutions significantly enhances diesel recovery compared to XG alone. For instance, adding 5 g/L SDS to 1 g/L XG achieved a recovery of 87.5 ± 1.2 %, while combining 5 g/L SDS with 2 g/L XG further improved recovery to 92.9 ± 0.8 %. As shown in Table 3, the addition of 5 g/L SDS to 1 g/L XG reduced the IFT with diesel by over twelve-fold, while its addition to 2 g/L XG resulted in a sixteen-fold IFT reduction. This significant decrease in IFT is the primary mechanism driving enhanced diesel recovery, as it facilitates the mobilization of contaminants by reducing the capillary forces between the two immiscible phases. However, deespite these improvements, residual diesel ganglia remain trapped within pore spaces after flushing with XG and XG + SDS solutions, hindering further mobilization and recovery.

Notably, the emulsion demonstrated the highest diesel recovery, achieving 100 %. Therefore, the key mechanisms contributing to this complete diesel recovery include: (i) high viscosity coupled with shear-thinning rheology (Fig. 2), (ii) significant IFT reduction between the aqueous and organic phases due to the presence of SDS and 1-pentanol (Table 3), and (iii) the swelling mechanism of the diesel phase induced by 1-pentanol. The emulsion's high viscosity and shear-thinning behavior facilitate stable and uniform displacement within porous media. Its shear-thinning rheology ensures that viscosity decreases under shear stress during injection but increases under low-shear conditions in porous media, preventing premature phase separation and maintaining droplet integrity. Additionally, the presence of SDS as a surfactant stabilizes the dispersed 1-pentanol phase by forming a protective interfacial film around the droplets, effectively reducing IFT and preventing coalescence. Meanwhile, the biopolymer XG enhances the emulsion's colloidal stability by increasing the viscoelasticity of the continuous phase, thereby retarding the creaming mechanism that could otherwise lead to emulsion instability [20]. Bulk experiments in graduated cylinders further confirm the long-term stability of the emulsion, showing that it remains stable for at least 30 days [66]. As a result, the emulsion exhibits high stability under dynamic flow conditions in porous media, driven by the viscosity of the continuous phase and the electrostatic repulsion between dispersed 1-pentanol droplets induced by SDS. This stability ensures the effective transport of dispersed 1-pentanol droplets into low-permeability zones, where they facilitate diesel mobilization and enhance recovery.

The high recovery efficiency of the emulsion is primarily attributed to the physicochemical interactions between 1-pentanol and diesel, which facilitate diesel ganglia swelling and mobilization during emulsion injection. Due to its longer hydrophobic alkyl chain, 1-pentanol preferentially partitions into the diesel phase rather than the aqueous phase, significantly altering the physicochemical properties of the trapped diesel ganglia [66]. This partitioning induces two key mechanisms: swelling of diesel ganglia and a reduction in IFT, both of which contribute to enhanced diesel displacement. The swelling mechanism occurs when 1-pentanol partitions into the diesel phase, disrupting intermolecular forces and causing the ganglia to expand in volume. This expansion reduces the capillary forces that trap diesel within soil pores, making it easier to mobilize [11]. As a result, previously immobile diesel becomes more connected, enhancing its displacement efficiency. Additionally, 1-pentanol lowers the IFT between the aqueous and diesel phases, further enhancing diesel mobilization. The combined effects of swelling and IFT reduction leads to an overall improvement in diesel connectivity and flowability, enabling the emulsion to displace diesel more effectively, particularly in low-permeability zones. Consequently, the diesel swelling mechanism induced by 1-pentanol plays a crucial role in enhancing recovery efficiency and will be further examined through effluent sample refractometry in Section 3.3.3. Following the injection of 1.2 PV, RF plateaued across all fluids, indicating no further significant changes in diesel recovery.

Fig. 4b illustrates the pressure gradient results as a function of PV in 1D sand-pack column for various injection fluids during diesel recovery. While all fluids achieved similar diesel recovery factors before breakthrough, their pressure gradient profiles exhibited notable differences. Increasing the XG concentration in polymer-only solutions significantly elevated the pressure gradient, with a twofold rise observed when the XG concentration was doubled. This increase is attributed to the higher viscosity of the 2 g/L XG solution, which enhances displacement due to the greater resistance to flow.

The addition of SDS (5 g/L) to XG solutions (1 g/L and 2 g/L) significantly reduced IFT between the aqueous and organic phases (see Table 3), resulting in lower pressure gradients compared to polymer-only solutions. For the 1 g/L XG + 5 g/L SDS solution, the reduced pressure gradient relative to the polymer-only 1 g/L XG solution can also be attributed to its lower viscosity, as confirmed by bulk rheological measurements (see Section 3.1.1). In contrast, no significant changes in viscosity were observed between the 2 g/L XG and 2 g/L XG + 5 g/L SDS solutions (see Fig. 2). As a result, the decrease in the pressure gradient for the 2 g/L XG + 5 g/L SDS solution, compared to the polymer-only 2 g/L XG solution, is primarily associated with the reduction in IFT during two-phase flow in porous media rather than changes in viscosity. The latter mechanisms, driven by SDS, facilitate diesel mobilization through IFT reduction rather than solubilization or in-situ emulsion formation.

Interestingly, the emulsion demonstrated a moderate pressure gradient, slightly higher than that of the 1 g/L XG solution, yet significantly lower than the high-viscosity 2 g/L XG solution, which exhibited the highest pressure gradient due to its increased viscosity. Despite its relatively low pressure gradient, the emulsion achieved a 100 % diesel recovery, surpassing the performance of all other injection fluids. This balance between a minimal pressure gradient and high recovery efficiency underscores the emulsion's effectiveness in displacing diesel from soil. From an application perspective, the lower pressure gradient associated with the emulsion enables easier injection into soil during diesel remediation scenarios, thereby reducing energy demands and operational complexity. These results highlight the emulsion's significant advantages for soil remediation, combining high removal efficiency with practical applicability.

3.3.2. *Effect of emulsion post-injection on diesel recovery*

In real-field remediation of LNAPL-contaminated soils, the pump-and-treat (PT) technique the commonly employed as a primary step to recover free-phase LNAPL product [15]. To mimic this approach, the post-treatment experiments were performed using a sequential manner, starting with waterflooding (WF) as the initial step, followed by emulsion injection. Fig. 5 depicts the diesel recovery efficiency as a function of PV during emulsion post-injection across four comparable experiments (Column 1–4) conducted in 1D sand-packed columns. The waterflooding phase primarily targeted the removal of free diesel product, mimicking the pump-and-treat technique. To assess the influence of diesel residual saturation on the efficiency of the emulsion injection, column experiments were conducted, resulting in varied residual diesel saturations. Recovery factors during the waterflooding

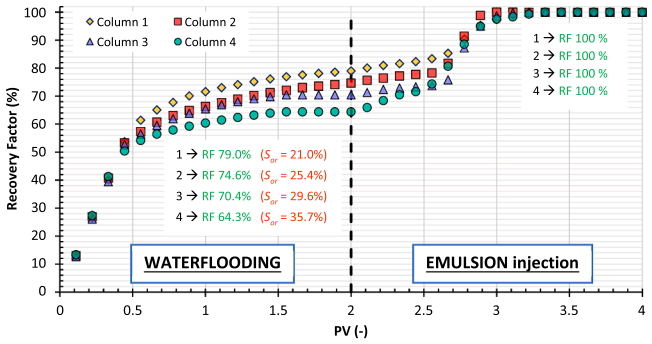

Fig. 5. Diesel recovery efficiency as a function of PV in 1D sand-pack columns during emulsion post-injection.

phase ranged from 64.3 % under less favorable conditions to 79 % under optimal conditions, corresponding to residual saturations of 35.7 %, 29.6 %, 25.4 %, and 21 %, respectively. These variations highlight the impact of grain size and column packing on diesel displacement. The limited recovery observed at waterflooding stage is primarily attributed to flow instability driven by capillary and viscous fingering, as explained in Section 3.2 using Lenormand's phase diagram. This instability hinders efficient displacement within the porous media, leading to bypassing of low-permeability zones where residual diesel remains trapped. Beyond approximately 2 PV of water injection, no further diesel recovery was achieved, indicating the inherent limitations of conventional waterflooding techniques in overcoming capillary forces and achieving complete remediation.

The post-injection of emulsion following waterflooding demonstrated high efficiency, achieving 100 % diesel recovery across all columns within 1.2–1.3 PV, regardless of the initial residual diesel saturations. These results highlight the emulsion's ability to overcome the limitations of conventional waterflooding, such as incomplete recovery caused by capillary forces and heterogeneities in porous media. Through a combination of oil-swelling and mobilization mechanisms, the emulsion effectively displaced the residual diesel ganglia that remained trapped after waterflooding. The diesel swelling mechanism and its role in enhancing recovery efficiency are comprehensively discussed in Section 3.3.3. Notably, the final recovery efficiency was independent of the initial residual saturation, further highlighting the emulsion's effectiveness as an enhanced remediation fluid for diesel-contaminated soils.

Fig. 6 presents the pressure gradient results as a function of PV for emulsion post-injection experiments conducted after the waterflooding phase. The corresponding pressure gradient trends during waterflooding phase for diesel recovery are provided in Figure S. 2 (see Supporting Data S4). During emulsion injection, the pressure gradients in all four

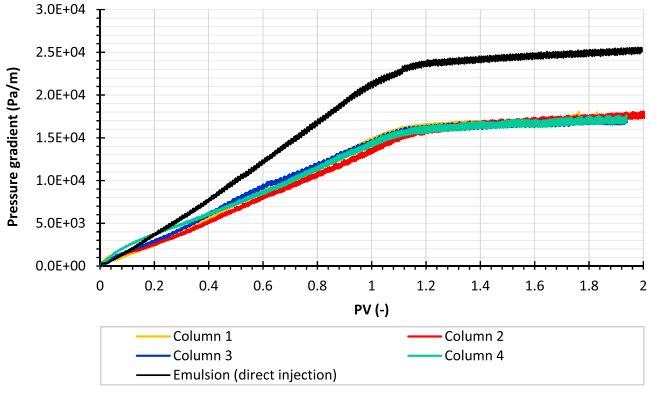

Fig. 6. Pressure gradient profiles as a function of PV in 1D sand-pack columns: Emulsion post-injection results compared to direct emulsion injection.

post-injection columns (yellow, red, blue, and green lines) increased steadily with PV, demonstrating comparable behavior despite slight variations due to differences in initial residual diesel saturation. All columns exhibited a gradual increase in pressure gradient until reaching a plateau near 1.3 PV, which corresponds to complete diesel recovery (100 %). This plateau reflects the emulsion's ability to efficiently displace residual diesel without causing excessive resistance to flow, even under differing diesel saturation conditions.

In Fig. 6, we have also compared the pressure gradients observed during emulsion post-injection experiments after waterflooding and direct emulsion injection (Fig. 4b). In contrast to post-injection experiments, where waterflooding reduced diesel saturation prior to emulsion application, the direct injection of the emulsion into a fully diesel-saturated porous medium with only 17 % irreducible water saturation (black line) exhibited a notably higher pressure gradient. The pressure gradient for direct injection increased more sharply with PV and remained consistently higher throughout the injection process compared to post-injection columns. This behavior is attributed to the higher initial diesel saturation in the direct injection scenario, which introduces greater capillary forces, thereby requiring higher pressure to mobilize the diesel. Although both strategies reached a plateau near 1.3 PV, the pressure gradient beyond the plateau during direct injection was approximately 1.5 times higher than those observed in the post-injection columns. Despite this difference, the 1.5-fold increase in the pressure gradient remains moderate compared to other highly viscous shear-thinning fluids.

The emulsion demonstrated exceptional diesel recovery efficiency in 1D sand-packed columns, achieving 100 % recovery within approximately 1.3 PV of injection in both direct and post-waterflooding scenarios. This finding suggests that, in field applications, the emulsion could be directly injected without requiring a preliminary pump-and-treat or waterflooding step, achieving similarly high recovery factors with comparable PV injections. Such an approach offers significant economic advantages by reducing the operational costs and time associated with the pump-and-treat phase. However, it is essential to note that these results were obtained under controlled laboratory conditions using 1D column experiments. To ensure the feasibility and scalability of emulsion injection in real-world remediation, further research is required at larger scales, including 2D tanks, 3D reservoirs, and pilot-scale systems. These investigations would provide deeper insights into the emulsion's performance in complex and heterogeneous environments, bridging the gap between laboratory findings and practical field applications.

3.3.3. Influence of oil-swelling alcohol on emulsion performance in diesel recovery

This section examines the role of oil-swelling alcohol in enhancing the emulsion's performance for diesel recovery. The analysis includes effluent characterization using refractometry and an examination of the relationship between residual NAPL saturation (S_{or}) and the capillary number (Ca). The influence of oil-swelling alcohol on the diesel displacement mechanism in 1D sand-packed columns was analyzed for both injection scenarios: direct emulsion injection and emulsion post-injection after waterflooding. This comprehensive assessment combines (a) visual tracking of the displacement front as a function of PV and (b) effluent refractometry measurements to quantify diesel recovery and analyze phase composition.

Fig. 7 presents the results of the direct injection of the emulsion into a fully diesel-saturated porous medium with an irreducible water saturation (S_{wi}) of 17 %. The photos of the column (Fig. 7a) show the stable and uniform propagation of the emulsion front, which attributed to its high viscosity and shear-thinning rheology. This behavior aligns with the higher viscosity ratio (M), as described in Section 3.2, contributing to efficient diesel displacement. Complete diesel recovery was achieved within 1.2 PV of emulsion injection, as evidenced by the second-to-last photo in the series.

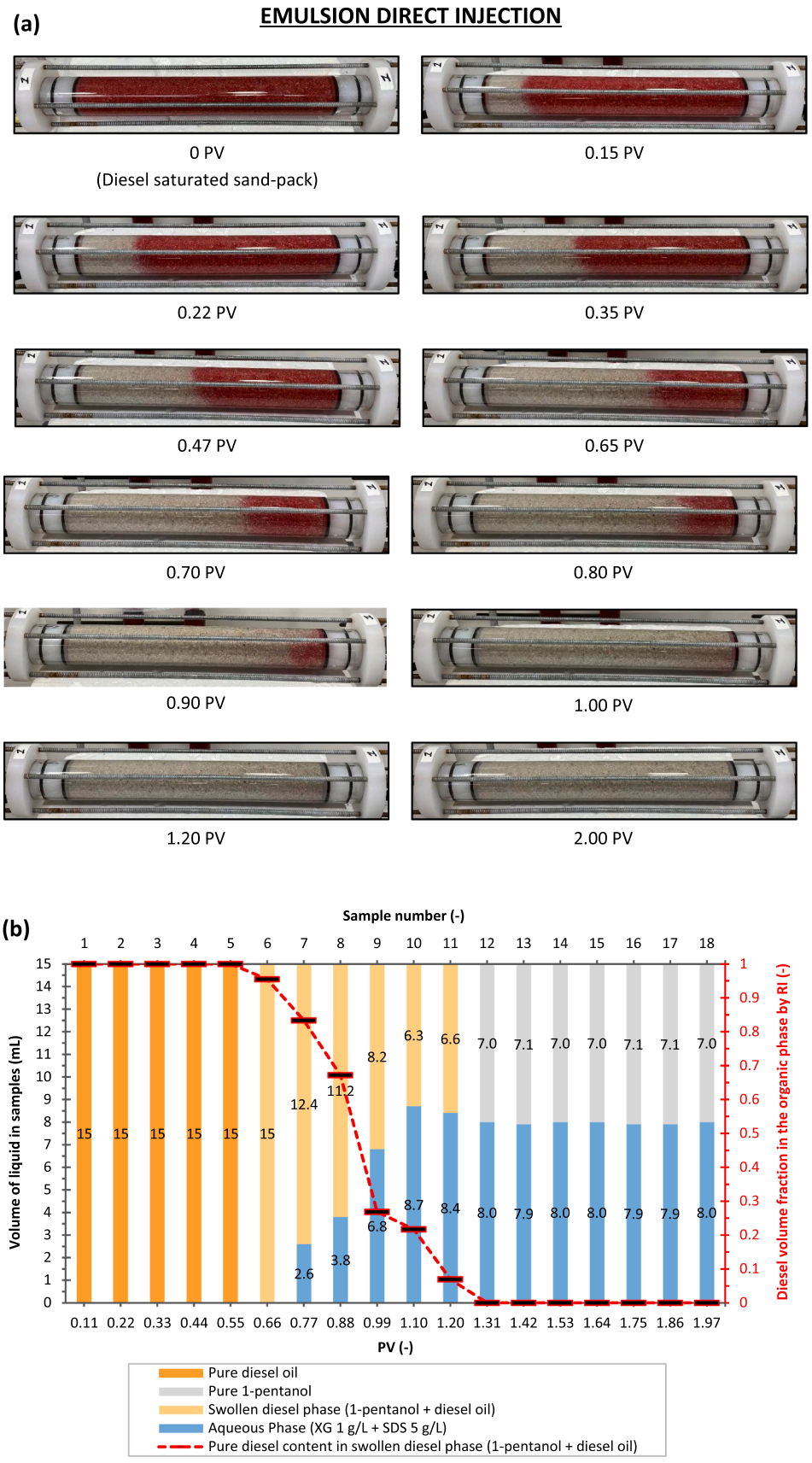

Fig. 7. Diesel displacement behavior in a 1D sand-pack column during direct emulsion injection: (a) visual progression as a function of PV and (b) corresponding effluent sample analysis using a refractometer, illustrating composition and diesel recovery.

Effluent sample analysis (Fig. 7b) complements these observations, revealing a consistent recovery trend. The first five samples (1−5) consist of pure diesel, effectively displaced by the viscous emulsion. Starting from sample 6 (0.66 PV), refractometer measurements confirmed the presence of 1-pentanol in the effluent, indicating its partitioning into the diesel phase within the porous medium. This partitioning at the emulsion-diesel interface caused a swelling mechanism that subsequently facilitated the mobilization of diesel. Notably, although the emulsion front had not yet reached the column outlet at 0.66 PV (as shown in Fig. 7a), the early detection of 1-pentanol in the effluent highlights its partitioning ability and transport. The swelling mechanism enhanced diesel recovery, as shown by the gradual decrease in diesel volume fraction (red dashed line) in the organic phase of samples 6–11. By sample 12 (1.31 PV), the diesel volume fraction in the effluent reached zero, confirming 100 % diesel recovery. The remaining organic phase consisted solely of 1-pentanol, further validating the emulsion's efficiency to achieve complete diesel displacement. The combination of the emulsion's shear-thinning rheology and the swelling mechanism induced by 1-pentanol proved highly effective in mobilizing and recovering diesel.

Fig. 8 presents the results of emulsion post-injection after the waterflooding process for "Column 1", as discussed in Section 3.3.2. The results for the other three columns (Columns 2, 3, and 4) showed the same behavior (see Supporting Data S5, Figure S. 3 and S. 4). The visual progression of water injection as a function of PV for "Column 1" is shown in Figure S. 3a (see Supporting Data S5), showing the gradual displacement of diesel during waterflooding, which left behind a residual diesel saturation. Following the waterflooding phase, the emulsion post-injection demonstrated stable and uniform propagation through the porous medium, as seen in the photos of Fig. 8a. This behavior can be attributed to the emulsion's viscosity and shear-thinning rheology (Fig. 2), which facilitated the targeted delivery of dispersed 1-pentanol droplets into low-permeability zones, effectively mobilizing trapped diesel residuals. Unlike the direct injection case, where the column was fully saturated with diesel, the initial condition for emulsion post-injection (Column 1) corresponded to a residual diesel saturation (S_{or}) of 21 % after 2 PV of waterflooding.

According to Fig. 8b the first five samples (1−5) demonstrate the displacement of both water and pure diesel residuals, driven by the emulsion's high viscosity, which effectively mobilized trapped diesel. Starting from sample 6 (after 0.55 PV of injection), refractometer measurements confirmed the presence of 1-pentanol in the effluent, indicating its partitioning into the diesel phase. Despite the emulsion front not yet reaching the column outlet at 0.66 PV (see Fig. 8a), the early detection of 1-pentanol highlights its ability to swell residual diesel ganglia, transitioning them into a recoverable phase. This observation aligns with the findings of [11], who reported that partitioning alcohols swell and transition residual DNAPL droplets into a continuous phase, making them easier to mobilize compared to disconnected residuals.

When the 1-pentanol-containing emulsion comes into contact with residual diesel ganglia within the porous medium, it breaks down at the interface, enabling the partitioning of 1-pentanol into the diesel phase. This process enhances diesel recovery by initiating a swelling mechanism, converting previously immobile diesel ganglia into a continuous, mobilizable phase. As a result, complete diesel recovery (100 %) was achieved by overcoming capillary entrapment forces within just 1.31 PV of injection. From sample 13 onward, the diesel volume fraction (red dashed lien) in the organic phase of the effluent samples dropped to zero, highlighting the emulsion's effectiveness to achieve total diesel removal with minimal injection volumes.

Both Figs. 7 and 8 demonstrate the emulsion's effectiveness in achieving 100 % diesel recovery at similar PV injections, despite different initial conditions between the two experiments. Direct injection shows higher initial efficiency due to the absence of waterflooding step, enabling the emulsion to directly target and displace diesel from a fully saturated porous medium. In contrast, post-injection focuses on mobilizing residual diesel left behind after waterflooding.

Fig. 9 shows the relationship between residual NAPL saturation (S_{or}) and the capillary number (Ca) for various injection fluids tested in this study, including waterflooding, polymer solutions, polymer-surfactant solutions, and the emulsion. For comparative analysis, data from recent studies by Bouzid et al. [10] and Omirbekov et al. [55] are also included. The study by Omirbekov et al. [55] investigated the removal of chlorinated organic hydrocarbons (DNAPL) from glass bead-packed porous media ($k = 227$ μm^2) using three different polymer solutions: 1 g/L xanthan gum (XG), 3 g/L guar gum (GG) and 4 g/L carboxymethyl cellulose (CMC). Bouzid et al. [10] analyzed polymer solutions of 2 g/L XG with and without addition of sodium dodecylbenzene sulfonate (SDBS) surfactant at a concentration of 0.94 g/L (equivalent to 1.3 × critical micelle concentration). Their study targeted the removal of the same chlorinated organic hydrocarbons from a permeability-contrasted sandbox ($k_1 = 13$ μm^2; $k_2 = 130$ μm^2).

The results of our experiments demonstrate that adding 1 g/L of XG polymer to deionized water enhanced diesel recovery, thereby reducing S_{or} by increasing the capillary number in the porous media from 6.10×10^{-7} ($S_{or} = 30.2 \pm 5.2$ %) for water alone to 1.62×10^{-4} ($S_{or} = 16.6 \pm 0.7$ %). Increasing the XG concentration from 1 g/L to 2 g/L further enhanced this effect, resulting in a threefold increase in Ca (from 1.62×10^{-4} to 4.88×10^{-4}) and a reduction in S_{or} to 11.7 ± 0.6 %, reflecting the impact of higher viscosity and improved displacement efficiency. Incorporating 5 g/L SDS into the 1 g/L and 2 g/L XG solutions further improved recovery by lowering the IFT between the aqueous and NAPL phases. This led to increased Ca values of 1.20×10^{-3} and 8.37×10^{-3}, respectively, and achieved even lower S_{or} of 12.5 ± 1.2 % and 7.1 ± 0.8 %. These results align with the general trend of decreasing S_{or} with increasing Ca, following the power-law relationship represented by the dashed blue line, consistent with findings by [10,14,37,46,55,60,16].

However, the behavior of the emulsion containing the oil-swelling alcohol 1-pentanol deviates significantly from the general power-law trend followed by other fluids, including those studied by Bouzid et al. [10] and Omirbekov et al. [55]. While these fluids rely on increasing Ca to achieve lower S_{or}, the emulsion achieves complete diesel recovery ($S_{or} = 0$ %) at relatively low Ca values. Specifically, the Ca for the emulsion ranged between 1.20×10^{-3} and 3.53×10^{-3} (green circles in Fig. 9), consistently reaching zero S_{or} across this range. This behavior highlights the unique displacement dynamics of the emulsion in NAPL-contaminated porous media, where the flow regime is neither fully miscible nor fully immiscible. Upon contact with diesel, the emulsion breaks down at the interface, allowing 1-pentanol droplets to partition into the diesel phase, causing swelling (a miscible interaction) that facilitates mobilization. Simultaneously, the viscous continuous aqueous phase of the emulsion (1 g/L XG + 5 g/L SDS) mobilizes the swollen diesel through immiscible displacement. This dual mechanism of miscible swelling and immiscible displacement means that the exact Ca cannot be represented by a single value and is instead positioned within the specified range. The interplay between the emulsion's miscible and immiscible behaviors is governed by the IFT between its continuous phase and both diesel oil and 1-pentanol (see Table 3). This unique combination allows the emulsion to efficiently mobilize and recover diesel, bypassing the need for higher capillary numbers.

The data from Bouzid et al. [10] and Omirbekov et al. [55] further highlights the clear advantages of the emulsion. While Bouzid et al.'s [10] use of 2 g/L XG + 0.94 g/L SDBS solution achieved S_{or} as low as 6.7 ± 0.5 %, and Omirbekov et al.'s [55] higher-concentration polymers (3 g/L GG and 4 g/L CMC) showed significant improvements in NAPL recovery, neither approach achieved complete residual NAPL removal ($S_{or} = 0$ %) as observed with the emulsion in this study. These findings highlight the significant interest of the emulsion proposed in this study compared to other shear-thinning fluids, making it a promising candidate for enhanced remediation strategies in complex subsurface environments.

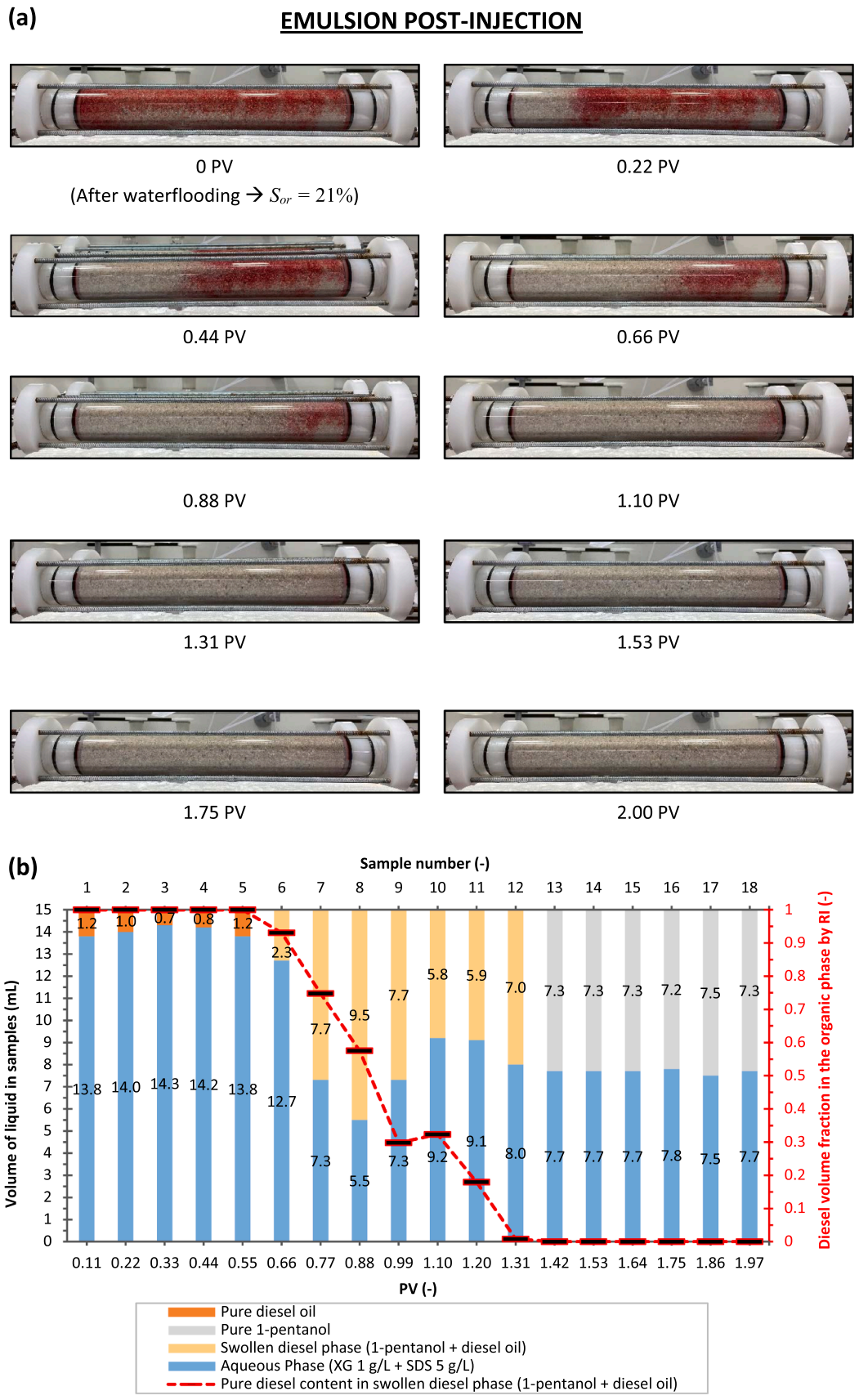

Fig. 8. Diesel displacement behavior during emulsion post-injection after waterflooding for the "Column 1": (a) visual progression as a function of PV, and (b) corresponding effluent sample analysis using a refractometer, illustrating composition and diesel recovery.

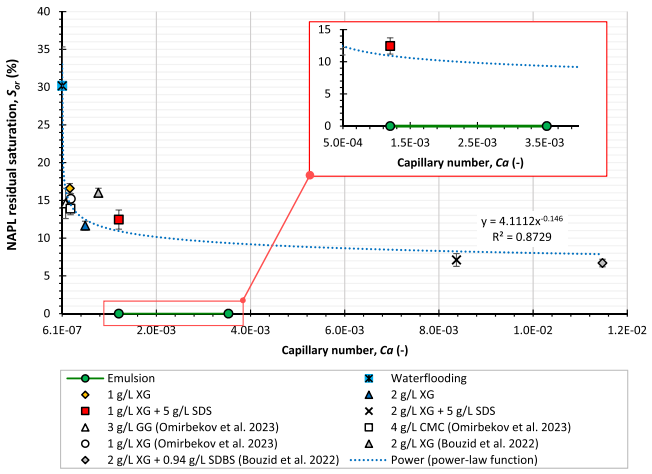

Fig. 9. Residual NAPL saturation in porous media as a function of capillary number.

4. Conclusions

In this study, we evaluated the performance of an alcohol-in-biopolymer emulsion for enhanced remediation of diesel-contaminated sandy soils. The emulsion, formulated with an aqueous continuous phase containing 1 g/L xanthan gum (XG) biopolymer and 5 g/L sodium dodecyl sulfate (SDS) surfactant, along with an organic dispersed phase of oil-soluble 1-pentanol in a 1:1 vol ratio, was tested in 1D sand-packed columns under direct injection and post-waterflooding scenarios. Bulk rheological experiments and interfacial tension (IFT) measurements provided insights into the emulsion's flow behavior and displacement mechanisms, while effluent refractometry highlighted the critical role of oil-swelling 1-pentanol in enhancing remediation efficiency. Hence, the key findings are summarized as follows:

- Rheological experiments confirmed that the emulsion exhibits highly viscous, non-Newtonian shear-thinning properties, ensuring stable and uniform propagation in porous media while efficiently delivering dispersed 1-pentanol droplets into low-permeability zones.
- The emulsion achieved 100 % diesel recovery in 1D sand-packed columns within just 1.2 PV of injection. This complete diesel recovery ($S_{or} = 0$) is attributed to three key mechanisms: (i) the high viscosity and shear-thinning properties of the emulsion, ensuring efficient displacement (as confirmed by the bulk rheological experiments), (ii) the significant reduction in IFT between the aqueous and organic phases, facilitated by the presence of SDS and 1-pentanol in the emulsion (as verified by IFT measurements), and (iii) the complete mobilization of diesel phase through the swelling mechanism induced by 1-pentanol (as evidenced by refractometry analysis of effluent samples).
- The emulsion outperformed other non-conventional polymer-only and polymer-surfactant solutions, achieving complete diesel recovery despite viscosity differences. While 1 g/L XG and 1 g/L XG + 5 g/L SDS solutions achieved recovery factors of 83.4 ± 0.7 % and 87.5 ± 1.2 %, and more viscous solutions like 2 g/L XG and 2 g/L XG + 5 g/L SDS achieved 88.3 ± 0.6 % and 92.9 ± 0.8 %, respectively, none matched the emulsion's complete recovery efficiency. Furthermore, the emulsion required lower pressure gradients – approximately two times lower than the highly viscous 2 g/L XG solution – demonstrating easier injectability with reduced energy demands and operational complexity.
- Unlike previous studies that correlate decreasing residual NAPL saturation (S_{or}) with increasing capillary number (Ca), the emulsion achieved zero S_{or} even at low Ca. This deviation from the general trend is attributed to the diesel swelling mechanism induced by 1-pentanol, which bypasses traditional capillary number constraints, highlighting the emulsion's unique and effective displacement dynamics.
- The emulsion achieved 100 % diesel recovery within 1.3 PV during post-injection after waterflooding. These experiments demonstrated that regardless of the residual diesel saturation left after waterflooding technique, the emulsion effectively sweeps and mobilizes all diesel ganglia within the same injection volume. This efficiency is also explained by the swelling mechanism, wherein 1-pentanol partitions into residual diesel droplets, causing them to swell and transition into a continuous phase that is more easily mobilized compared to disconnected residuals.

These findings suggest that combining a diesel-swelling alcohol with a shear-thinning biopolymer-surfactant solution into a single flushing emulsion is a highly effective approach for the enhanced remediation of diesel-contaminated soils. To further validate its practical applicability, future large-scale studies, such as 2D and 3D tank experiments, are essential to assess scalability and confirm its effectiveness in real-world remediation scenarios. Such investigations will provide deeper insights into the emulsion's performance in complex subsurface environments, ensuring its effectiveness beyond controlled laboratory conditions. Additionally, key factors influencing emulsion effectiveness — including long-term stability under varying storage durations and temperature conditions, as well as subsurface heterogeneity characterized by clay and organic matter content and permeability contrasts in multilayer soil systems — should be thoroughly evaluated. Addressing these aspects will help refine the emulsion formulation and optimize the injection strategy for efficient and sustainable large-scale remediation applications.

Environmental implication

Contamination of soils and aquifers by petroleum hydrocarbons poses significant risks to environmental sustainability and public health. This study introduces a novel emulsion as an innovative solution for the enhanced remediation of diesel-contaminated soils. Formulated with biodegradable and environmentally friendly components - xanthan gum, sodium dodecyl sulfate, and 1-pentanol - the emulsion significantly enhances diesel recovery while minimizing environmental impact. Its shear-thinning properties ensure stable pollutant displacement, and the oil-swelling mechanism induced by 1-pentanol facilitates complete diesel removal. This novel approach represents a significant advancement over conventional and unconventional remediation techniques, contributing to more sustainable soil and groundwater remediation practices.

CRediT authorship contribution statement

Krimissa Mohamed: Visualization, Validation, Supervision, Resources, Funding acquisition. **Lorthioy Mélanie:** Visualization, Validation, Supervision, Resources, Funding acquisition. **Dicharry Christophe:** Writing – review & editing, Validation, Supervision, Methodology, Investigation, Conceptualization. **Sabyrbay Bexultan:** Writing – original draft, Visualization, Validation, Software, Methodology, Investigation, Formal analysis, Data curation, Conceptualization. **Colombano Stéfan:** Writing – review & editing, Validation, Supervision, Project administration, Methodology, Funding acquisition, Conceptualization. **Davarzani Dorian:** Writing – review & editing, Validation, Supervision, Methodology, Conceptualization. **Kodebay Iliyas:** Validation, Investigation. **Omirbekov Sagyn:** Writing – review & editing, Validation, Methodology, Investigation, Conceptualization.

Declaration of Competing Interest

The authors declare that they have no known competing financial

interests or personal relationships that could have appeared to influence the work reported in this paper.

Acknowledgements

This study was carried out as part of the "MOBILMOUSSE" project. The authors would like to thank BRGM (the French Geological Survey), EDF (Électricité de France), COLAS ENVIRONNEMENT, and ANRT (Association Nationale de la Recherche et de la Technologie) for co-financing the project. We also acknowledge the financial support of the PIVOTS project from the "Région Centre-Val de Loire" and the European Regional Development Fund.

Appendix A. Supporting information

Supplementary data associated with this article can be found in the online version at doi:10.1016/j.jhazmat.2025.138183.

Data availability

The data that has been used is confidential.

References

[1] Alamooti, A., Colombano, S., Glabe, Z.A., Lion, F., Davarzani, D., Ahmadi-Sénichault, A., 2023. Remediation of multilayer soils contaminated by heavy chlorinated solvents using biopolymer-surfactant mixtures: Two-dimensional flow experiments and simulations. Water Res 243, 120305. https://doi.org/10.1016/j.watres.2023.120305.

[2] Atteia, O., Del Campo Estrada, E., Bertin, H., 2013. Soil flushing: A review of the origin of efficiency variability. Rev Environ Sci Bio/Technol 12 (4), 379–389. https://doi.org/10.1007/s11157-013-9316-0.

[3] Aydin, G.A., Agaoglu, B., Kocasoy, G., Copty, N.K., 2011. Effect of temperature on cosolvent flooding for the enhanced solubilization and mobilization of NAPLs in porous media. J Hazard Mater 186 (1), 636–644. https://doi.org/10.1016/j.jhazmat.2010.11.046.

[4] Babeu, L., Vaishnav, D.D., 1987. Prediction of biodegradability for selected organic chemicals. J Ind Microbiol 2 (2), 107–115. https://doi.org/10.1007/BF01569509.

[5] Baigadilov, A., Colombano, S., Omirbekov, S., Cochennec, M., Davarzani, D., Lion, F., et al., 2024. Surfactant foam injection for remediation of diesel-contaminated soil: a comprehensive study on the role of co-surfactant in foaming formulation enhancement. Sci Total Environ 930, 172631. https://doi.org/10.1016/j.scitotenv.2024.172631.

[6] Baigadilov, A., Colombano, S., Omirbekov, S., Cochennec, M., Davarzani, D., Lion, F., et al., 2025. Stability and flow behavior of polymer-enhanced foams for improved in-situ remediation of hydrocarbons: Effect of polymer-surfactant interactions. J Hazard Mater 486, 137004. https://doi.org/10.1016/j.jhazmat.2024.137004.

[7] Batikh, A., Colombano, S., Cochennec, M., Davarzani, D., Perrault, A., Lions, J., et al., 2025. Mobilization of poly- and perfluoroalkyl substances (PFAS) from heterogeneous soils: desorption by ethanol/xanthan gum mixture. J Hazard Mater 481, 136496. https://doi.org/10.1016/j.jhazmat.2024.136496.

[8] Bernardez, L.A., De Andrade Lima, L.R.P., 2021. Microemulsions for remediation of light non-aqueous-phase liquids in aquifer rocks. Environ Earth Sci 80 (7), 257. https://doi.org/10.1007/s12665-021-09548-z.

[9] Bettahar, M., Ducreux, J., Schäfer, G., Dorpe, F.V., 1999. No title found. Transp Porous Media 37 (3), 255–276. https://doi.org/10.1023/A:1006634728321.

[10] Bouzid, I., Fatin-Rouge, N., 2022. Assessment of shear-thinning fluids and strategies for enhanced in situ removal of heavy chlorinated compounds-DNAPLs in an anisotropic aquifer. J Hazard Mater 432, 128703. https://doi.org/10.1016/j.jhazmat.2022.128703.

[11] Brandes, D., Farley, K.J., 1993. Importance of phase behavior on the removal of residual DNAPLs from porous media by alcohol flooding. Water Environ Res 65 (7), 869–878. https://doi.org/10.2175/WER.65.7.9.

[12] Charbeneau, R.J., Johns, R.T., Lake, L.W., McAdams, M.J., 2000. Free-Product Recovery of Petroleum Hydrocarbon Liquids. Groundw Monit Remediat 20 (3), 147–158. https://doi.org/10.1111/j.1745-6592.2000.tb00280.x.

[13] Chauveteau, G., & Zaitoun, A. (1981). Basic rheological behavior of xanthan polysaccharide solutions in porous media: Effects of pore size and polymer concentration. *Proceedings of the First European Symposium on Enhanced Oil Recovery, Bournemouth, England, Society of Petroleum Engineers, Richardson, TX*, 197–212.

[14] Colombano, S., Davarzani, H., Van Hullebusch, E.D., Huguenot, D., Guyonnet, D., Deparis, J., et al., 2020. Thermal and chemical enhanced recovery of heavy chlorinated organic compounds in saturated porous media: 1D cell drainage-imbibition experiments. Sci Total Environ 706, 135758. https://doi.org/10.1016/j.scitotenv.2019.135758.

[15] Colombano, S., Davarzani, H., Van Hullebusch, E.D., Ignatiadis, I., Huguenot, D., Omirbekov, S., et al., 2020. In: Van Hullebusch, E.D., Huguenot, D., Pechaud, Y., Simonnot, M.-O., Colombano, S. (Eds.), Free Product Recovery of Non-aqueous Phase Liquids in Contaminated Sites: Theory and Case Studies, *Environmental Soil Remediation and Rehabilitation*. Springer International Publishing, pp. 61–148. https://doi.org/10.1007/978-3-030-40348-5_2.

[16] Colombano, S., Davarzani, H., Van Hullebusch, Huguenot, D., Guyonnet, D., Deparis, J., Ignatiadis, I., 2021. Comparison of thermal and chemical enhanced recovery of DNAPL in saturated porous media: 2D tank pumping experiments and two-phase flow modelling. Sci. Total Environ. 760, 143958. https://doi.org/10.1016/j.scitotenv.2020.143958.

[17] Darby, R., Darby, R., Chhabra, R.P., 2017. Chemical Engineering Fluid Mechanics, Revised and Expanded, 0 ed.). CRC Press. https://doi.org/10.1201/9781315274492.

[18] Davarzani, D., Derikvand, Z., Betelu, S., Colombano, S., Nascimento, M., Ignatiadis, I., et al., 2024. Biopolymer-enhanced delivery of reactive sulfide reagents for in-situ mercury remediation of heterogeneous contaminated soils. Sci Total Environ 949, 174901. https://doi.org/10.1016/j.scitotenv.2024.174901.

[19] Demetriades, K., Julian McClements, D., 2000. Influence of sodium dodecyl sulfate on the physicochemical properties of whey protein-stabilized emulsions. Colloids Surf A: Physicochem Eng Asp 161 (3), 391–400. https://doi.org/10.1016/S0927-7757(99)00210-1.

[20] Dickinson, E., Ma, J., Povey, M.J.W., 1994. Creaming of concentrated oil-in-water emulsions containing xanthan. Food Hydrocoll 8 (5), 481–497. https://doi.org/10.1016/S0268-005X(09)80090-8.

[21] Dwarakanath, V., Kostarelos, K., Pope, G.A., Shotts, D., Wade, W.H., 1999. Anionic surfactant remediation of soil columns contaminated by nonaqueous phase liquids. J Contam Hydrol 38 (4), 465–488. https://doi.org/10.1016/S0169-7722(99)00006-6.

[22] Falta, R.W., 1998. Using Phase Diagrams to Predict the Performance of Cosolvent Floods for NAPL Remediation. Groundw Monit Remediat 18 (3), 94–102. https://doi.org/10.1111/j.1745-6592.1998.tb00733.x.

[23] Feng, S.-J., Niu, J.-G., Shi, F.-J., Zheng, Q.-T., Gao, M.-W., 2025. Remediation effectiveness and mechanism on surfactant-enhanced remediation of low-permeability petroleum hydrocarbon contaminated soil under fracturing conditions. J Hydrol 650, 132539. https://doi.org/10.1016/j.jhydrol.2024.132539.

[24] Forey, N., Atteia, O., Omari, A., Bertin, H., 2020. Saponin foam for soil remediation: on the use of polymer or solid particles to enhance foam resistance against oil. J Contam Hydrol 228, 103560. https://doi.org/10.1016/j.jconhyd.2019.103560.

[25] Fortin, J., Jury, W.A., Anderson, M.A., 1997. Enhanced removal of trapped non-aqueous phase liquids from saturated soil using surfactant solutions. J Contam Hydrol 24 (3–4), 247–267. https://doi.org/10.1016/S0169-7722(96)00013-7.

[26] Hernández-Espriú, A., Sánchez-León, E., Martínez-Santos, P., Torres, L.G., 2013. Remediation of a diesel-contaminated soil from a pipeline accidental spill: enhanced biodegradation and soil washing processes using natural gums and surfactants. J Soils Sediment 13 (1), 152–165. https://doi.org/10.1007/s11368-012-0599-5.

[27] Herring, A.L., Andersson, L., Schlüter, S., Sheppard, A., Wildenschild, D., 2015. Efficiently engineering pore-scale processes: The role of force dominance and topology during nonwetting phase trapping in porous media. Adv Water Resour 79, 91–102. https://doi.org/10.1016/j.advwatres.2015.02.005.

[28] Hofstee, C., Gutiérrez Ziegler, C., Trötschler, O., Braun, J., 2003. Removal of DNAPL contamination from the saturated zone by the combined effect of vertical upward flushing and density reduction. J Contam Hydrol 67 (1–4), 61–78. https://doi.org/10.1016/S0169-7722(03)00088-3.

[29] Javanbakht, G., Arshadi, M., Qin, T., Goual, L., 2017. Micro-scale displacement of NAPL by surfactant and microemulsion in heterogeneous porous media. Adv Water Resour 105, 173–187. https://doi.org/10.1016/j.advwatres.2017.05.006.

[30] Javanbakht, G., Goual, L., 2016. Impact of surfactant structure on NAPL mobilization and solubilization in porous media. Ind Eng Chem Res 55 (45), 11736–11746. https://doi.org/10.1021/acs.iecr.6b03006.

[31] Jawitz, J.W., Annable, M.D., Rao, P.S.C., Rhue, R.D., 1998. Field Implementation of a winsor type I Surfactant/alcohol mixture for in situ solubilization of a complex LNAPL as a single-phase microemulsion. Environ Sci Technol 32 (4), 523–530. https://doi.org/10.1021/es970507i.

[32] Jeong, S.-W., Ju, B.-K., Lee, B.-J., 2009. Effects of alcohol-partitioning type and airflow on cosolvent flooding to benzene-LNAPL saturated porous media. J Hazard Mater 166 (2–3), 603–611. https://doi.org/10.1016/j.jhazmat.2008.11.102.

[33] Karthick, A., Roy, B., Chattopadhyay, P., 2019. A review on the application of chemical surfactant and surfactant foam for remediation of petroleum oil contaminated soil. J Environ Manag 243, 187–205. https://doi.org/10.1016/j.jenvman.2019.04.092.

[34] Kibbey, T.C.G., Ramsburg, C.A., Pennell, K.D., Hayes, K.F., 2002. Implications of Alcohol Partitioning Behavior for In Situ Density Modification of Entrapped Dense Nonaqueous Phase Liquids. Environ Sci Technol 36 (1), 104–111. https://doi.org/10.1021/es010966q.

[35] Kozeny, J., 1927. ÜBer kapillare Leit Des Wassers Im Boden 136, 271. ⟨https://cir.nii.ac.jp/crid/1370285708268135431⟩.

[36] Krstonošić, V., Milanović, M., Dokić, L., 2019. Application of different techniques in the determination of xanthan gum-SDS and xanthan gum-Tween 80 interaction. Food Hydrocoll 87, 108–118. https://doi.org/10.1016/j.foodhyd.2018.07.040.

[37] Lake, L., Johns, R.T., Rossen, W.R., Pope, G.A., 1989. Fundamentals of Enhanced Oil Recovery. Society of Petroleum Engineers. https://doi.org/10.2118/9781613993286.

[38] Lee, K.Y., 2008. Phase partitioning modeling of ethanol, isopropanol, and methanol with BTEX compounds in water. Environ Pollut 154 (2), 320–329. https://doi.org/10.1016/j.envpol.2007.10.001.
[39] Lee, M., Kang, H., Do, W., 2005. Application of nonionic surfactant-enhanced in situ flushing to a diesel contaminated site. Water Res 39 (1), 139–146. https://doi.org/10.1016/j.watres.2004.09.012.
[40] Lenormand, R., Touboul, E., Zarcone, C., 1988. Numerical models and experiments on immiscible displacements in porous media. J Fluid Mech 189, 165–187. https://doi.org/10.1017/S0022112088000953.
[41] Liu, C., Kwon, J.-H., Prabhu, S.M., Ha, G.-S., Khan, M.A., Park, Y.-K., et al., 2022. Efficiency of diesel-contaminated soil washing with different tween 80 surfactant concentrations, pH, and bentonite ratios. Environ Res 214, 113830. https://doi.org/10.1016/j.envres.2022.113830.
[42] Liu, J.-W., Wei, K.-H., Xu, S.-W., Cui, J., Ma, J., Xiao, X.-L., et al., 2021. Surfactant-enhanced remediation of oil-contaminated soil and groundwater: a review. Sci Total Environ 756, 144142. https://doi.org/10.1016/j.scitotenv.2020.144142.
[43] Longpré-Girard, M., Martel, R., Robert, T., Lefebvre, R., Lauzon, J.-M., 2016. 2D sandbox experiments of surfactant foams for mobility control and enhanced LNAPL recovery in layered soils. J Contam Hydrol 193, 63–73. https://doi.org/10.1016/j.jconhyd.2016.09.001.
[44] Lunn, S.R.D., Kueper, B.H., 1997. Removal of pooled dense, nonaqueous phase liquid from saturated porous media using upward gradient alcohol floods. Water Resour Res 33 (10), 2207–2219. https://doi.org/10.1029/97WR01692.
[45] Mackay, D.M., Cherry, J.A., 1989. Groundwater contamination: Pump-and-treat remediation. Environ Sci Technol 23 (6), 630–636. https://doi.org/10.1021/es00064a001.
[46] Maire, J., Joubert, A., Kaifas, D., Invernizzi, T., Marduel, J., Colombano, S., et al., 2018. Assessment of flushing methods for the removal of heavy chlorinated compounds DNAPL in an alluvial aquifer. Sci Total Environ 612, 1149–1158. https://doi.org/10.1016/j.scitotenv.2017.08.309.
[47] Mao, X., Jiang, R., Xiao, W., Yu, J., 2015. Use of surfactants for the remediation of contaminated soils: a review. J Hazard Mater 285, 419–435. https://doi.org/10.1016/j.jhazmat.2014.12.009.
[48] Martel, R., Hébert, A., Lefebvre, R., Gélinas, P., Gabriel, U., 2004. Displacement and sweep efficiencies in a DNAPL recovery test using micellar and polymer solutions injected in a five-spot pattern. J Contam Hydrol 75 (1–2), 1–29. https://doi.org/10.1016/j.jconhyd.2004.03.007.
[49] Martel, K.E., Martel, R., Lefebvre, R., Gélinas, P.J., 1998. Laboratory Study of Polymer Solutions Used for Mobility Control During In Situ NAPL Recovery. Groundw Monit Remediat 18 (3), 103–113. https://doi.org/10.1111/j.1745-6592.1998.tb00734.x.
[50] Mazo Rivas, J.C., Schneider, Y., Rohm, H., 2016. Effect of emulsifier type on physicochemical properties of water-in-oil emulsions for confectionery applications. Int J Food Sci Technol 51 (4), 1026–1033. https://doi.org/10.1111/ijfs.13063.
[51] Milas, M., Rinaudo, M., Knipper, M., Schuppiser, J.L., 1990. Flow and viscoelastic properties of xanthan gum solutions. Macromolecules 23 (9), 2506–2511. https://doi.org/10.1021/ma00211a018.
[52] Mrokowska, M.M., Krztoń-Maziopa, A., 2019. Viscoelastic and shear-thinning effects of aqueous exopolymer solution on disk and sphere settling. Sci Rep 9 (1), 7897. https://doi.org/10.1038/s41598-019-44233-z.
[53] Nsengiyumva, E.M., Alexandridis, P., 2022. Xanthan gum in aqueous solutions: Fundamentals and applications. Int J Biol Macromol 216, 583–604. https://doi.org/10.1016/j.ijbiomac.2022.06.189.
[54] Okamura, M., Takebayashi, M., Nishida, K., Fujii, N., Jinguji, M., Imasato, T., Nakagawa, E., 2011. In-situ desaturation test by air injection and its evaluation through field monitoring and multiphase flow simulation. J. Geotech. Geoenviron. Eng. 137 (7), 643–652. https://doi.org/10.1061/(ASCE)GT.1943-5606.0000483.
[55] Omirbekov, S., Colombano, S., Alamooti, A., Batikh, A., Cochennec, M., Amanbek, Y., et al., 2023. Experimental study of DNAPL displacement by a new densified polymer solution and upscaling problems of aqueous polymer flow in porous media. J Contam Hydrol 252, 104120. https://doi.org/10.1016/j.jconhyd.2022.104120.
[56] Omirbekov, S., Davarzani, H., Ahmadi-Senichault, A., 2020. Experimental Study of Non-Newtonian Behavior of Foam Flow in Highly Permeable Porous Media. Ind Eng Chem Res 59 (27), 12568–12579. https://doi.org/10.1021/acs.iecr.0c00879.
[57] Omirbekov, S., Davarzani, H., Sabyrbay, B., Colombano, S., Ahmadi-Senichault, A., 2022. Experimental study of rheological behavior of foam flow in capillary tubes. J Non-Newton Fluid Mech 302, 104774. https://doi.org/10.1016/j.jnnfm.2022.104774.
[58] Pal, R., 1992. Rheology of polymer-thickened emulsions. J Rheol 36 (7), 1245–1259. https://doi.org/10.1122/1.550310.
[59] Paria, S., 2008. Surfactant-enhanced remediation of organic contaminated soil and water. Adv Colloid Interface Sci 138 (1), 24–58. https://doi.org/10.1016/j.cis.2007.11.001.
[60] Pennell, K.D., Pope, G.A., Abriola, L.M., 1996. Influence of viscous and buoyancy forces on the mobilization of residual tetrachloroethylene during surfactant flushing. Environ Sci Technol 30 (4), 1328–1335. https://doi.org/10.1021/es9505311.
[61] Primkulov, B.K., Pahlavan, A.A., Fu, X., Zhao, B., MacMinn, C.W., Juanes, R., 2021. Wettability and Lenormand's diagram. J Fluid Mech 923, A34. https://doi.org/10.1017/jfm.2021.579.
[62] Ramsburg, C.A., Pennell, K.D., Kibbey, T.C.G., Hayes, K.F., 2003. Use of a Surfactant-Stabilized Emulsion To Deliver 1-Butanol for Density-Modified Displacement of Trichloroethene. Environ Sci Technol 37 (18), 4246–4253. https://doi.org/10.1021/es0210291.
[63] Rhue, R.D., Rao, P.S.C., Annable, M.D., 1999. Single-Phase Microemulsification of a Complex Light-Nonaqueous-Phase-Liquid: Laboratory Evaluation of Several Mixtures of Surfactant/Alcohol Solutions. J Environ Qual 28 (4), 1135–1144. https://doi.org/10.2134/jeq1999.00472425002800040012x.
[64] Robert, T., Martel, R., Lefebvre, R., 2011. Use Intermed Scale Phys Model 3D situ Trials LNAPL Remediat Technol trains 8.
[65] Rosen, M.J., Kunjappu, J.T., 2012. Surfactants and interfacial phenomena. John Wiley & Sons.
[66] Sabyrbay, B., Davarzani, D., Dicharry, C., Omirbekov, S., Lion, F., Alamooti, A., et al., 2025. Assessment of a novel alcohol-in-biopolymer emulsion for enhanced remediation of diesel-contaminated soils. J Hazard Mater Adv 18, 100616. https://doi.org/10.1016/j.hazadv.2025.100616.
[67] Saenton, S., Illangasekare, T.H., Soga, K., Saba, T.A., 2002. Effects of source zone heterogeneity on surfactant-enhanced NAPL dissolution and resulting remediation end-points. J. Contam. Hydrol. 59 (1–2), 27–44. https://doi.org/10.1016/S0169-7722(02)00074-8.
[68] Sakhaei, Z., Riazi, M., 2022. In-situ petroleum hydrocarbons contaminated soils remediation by polymer enhanced surfactant flushing: mechanistic investigation. Process Saf Environ Prot 161, 758–770. https://doi.org/10.1016/j.psep.2022.03.086.
[69] Shiau, B.-J., Sabatini, D.A., Harwell, J.H., 2000. Chlorinated Solvent Removal Using Food Grade Surfactants: Column Studies. J Environ Eng 126 (7), 611–621. https://doi.org/10.1061/(ASCE)0733-9372(2000)126:7(611).
[70] Stauffer, C.E., 1965. The measurement of surface tension by the pendant drop technique. J Phys Chem 69 (6), 1933–1938. https://doi.org/10.1021/j100890a024.
[71] St-Pierre, C., Martel, R., Gabriel, U., Lefebvre, R., Robert, T., Hawari, J., 2004. TCE recovery mechanisms using micellar and alcohol solutions: phase diagrams and sand column experiments. J Contam Hydrol 71 (1–4), 155–192. https://doi.org/10.1016/j.jconhyd.2003.09.010.
[72] Stroo, H.F., Leeson, A., Marqusee, J.A., Johnson, P.C., Ward, C.H., Kavanaugh, M. C., Sale, T.C., Newell, C.J., Pennell, K.D., Lebrón, C.A., Unger, M., 2012. Chlorinated Ethene Source Remediation: Lessons Learned. Environ. Sci. Technol. 46 (12), 6438–6447. https://doi.org/10.1021/es204714w.
[73] Talawat, J., Sabatini, D.A., Tongcumpou, C., 2013. Behavior of DNAPL mixture of organometallic and chlorinated solvent in the presence of surfactants and alcohols as density modifying agents. J Environ Sci Health, Part A 48 (13), 1619–1627. https://doi.org/10.1080/10934529.2013.815093.
[74] Teige, G.M.G., Hermanrud, C., Thomas, W.H., Wilson, O.B., Nordgård Bolås, H.M., 2005. Capillary resistance and trapping of hydrocarbons: a laboratory experiment. Pet Geosci 11 (2), 125–129. https://doi.org/10.1144/1354-079304-609.
[75] Vaishnav, D.D., Boethling, R.S., Babeu, L., 1987. Quantitative structure—biodegradability relationships for alchols, ketones and alicyclic compounds. Chemosphere 16 (4), 695–703. https://doi.org/10.1016/0045-6535(87)90005-1.
[76] Wang, J., Li, J., Li, Y., Xu, R., Xu, G., Yang, J., 2024. Research on the influence of heterogeneity and viscosity on the fluid intrusion mechanism of the water flooding process based on the microscopic visualization experiment. ACS Omega 9 (2), 2866–2873. https://doi.org/10.1021/acsomega.3c08205.
[77] Wu, B., Zhang, Y., Zhang, X.-X., Cheng, S.-P., 2011. Health risk assessment of polycyclic aromatic hydrocarbons in the source water and drinking water of China: quantitative analysis based on published monitoring data. Sci Total Environ 410–411, 112–118. https://doi.org/10.1016/j.scitotenv.2011.09.046.
[78] Xu, Q., Chen, J., Wang, Y., Ke, S., 2022. Quantitative analysis of dominant mechanisms in improving fluid sweeping uniformity in a layered heterogeneous system via xanthan gum addition. Environ Sci Pollut Res 29 (17), 25759–25773. https://doi.org/10.1007/s11356-021-17632-x.
[79] Yang, W., Brownlow, J.W., Walker, D.L., Lu, J., 2021. Effect of Surfactant-Assisted Wettability Alteration on Immiscible Displacement: A Microfluidic Study. Water Resour Res 57 (8), e2020WR029522. https://doi.org/10.1029/2020WR029522.
[80] Yasuda, K., Armstrong, R.C., Cohen, R.E., 1981. Shear flow properties of concentrated solutions of linear and star branched polystyrenes. Rheol Acta 20 (2), 163–178. https://doi.org/10.1007/BF01513059.
[81] Zhao, X., Chen, B., Liu, T., Cai, Y., Huang, L., Zhao, M., et al., 2023. The formation, structural and rheological properties of emulsion gels stabilized by egg white protein-insoluble soybean fiber complex. Food Hydrocoll 134, 108035. https://doi.org/10.1016/j.foodhyd.2022.108035.
[82] Zhao, B., Li, S., Lin, H., Cheng, Y., Kong, X., Ding, Y., 2022. Experimental study on the influence of surfactants in compound solution on the wetting-agglomeration properties of bituminous coal dust. Powder Technol 395, 766–775. https://doi.org/10.1016/j.powtec.2021.10.026.
[83] Zhao, Y., Zhao, L., Chang, G., Chen, H., Hao, L., Zhao, N., et al., 2022. Fabrication of surfactant-biopolymer combined system with dual viscosity reduction and mobility controllability for heavy oil reservoirs. J Mol Liq 368, 120777. https://doi.org/10.1016/j.molliq.2022.120777.
[84] Zheng, L., Yoon, S., Ronan, A.D., 2012. Remediation of gasoline contaminated soil using surfactant enhanced aquifer remediation (SEAR). World Environ Water Resour Congr 2012 136–145. https://doi.org/10.1061/9780784412312.015.
[85] Zhong, L., Oostrom, M., Truex, M.J., Vermeul, V.R., Szecsody, J.E., 2013. Rheological behavior of xanthan gum solution related to shear thinning fluid delivery for subsurface remediation. J Hazard Mater 244–245, 160–170. https://doi.org/10.1016/j.jhazmat.2012.11.028.
[86] Zhong, L., Oostrom, M., Wietsma, T.W., Covert, M.A., 2008. Enhanced remedial amendment delivery through fluid viscosity modifications: experiments and

numerical simulations. J Contam Hydrol 101 (1–4), 29–41. https://doi.org/10.1016/j.jconhyd.2008.07.007.

[87] Zhong, L., Oostrom, M., 2012. LNAPL removal from unsaturated porous media using surfactant infiltration. Vadose Zone J 11 (4), vzj2011.0166. https://doi.org/10.2136/vzj2011.0166.

[88] Zhong, L., Szecsody, J., Oostrom, M., Truex, M., Shen, X., Li, X., 2011. Enhanced remedial amendment delivery to subsurface using shear thinning fluid and aqueous foam. J Hazard Mater 191 (1–3), 249–257. https://doi.org/10.1016/j.jhazmat.2011.04.074.